ADVANCED MATERIALS
www.advmat.de

Challenges and Opportunities of Upconversion Nanoparticles for Emerging NIR Optoelectronic Devices

Sunyingyue Geng, Hangfei Li, Ziyu Lv, Yongbiao Zhai, Bobo Tian, Ying Luo, Ye Zhou, and Su-Ting Han**

Upconversion nanoparticles (UCNPs), incorporating lanthanide (Ln) dopants, can convert low-energy near-infrared photons into higher-energy visible or ultraviolet light through nonlinear energy transfer processes. This distinctive feature has attracted considerable attention in both fundamental research and advanced optoelectronics. Challenges such as low energy-conversion efficiency and nonradiative losses limit the performance of UCNP-based optoelectronic devices. Recent advancements including optimized core–shell structures, tailed Ln-doping concentration, and surface modifications show significant promise for improving the efficiency and stability. In addition, combining UCNPs with functional materials can broaden their applications and improve device performance, paving the way for the innovation of next-generation optoelectronics. This paper first categorizes and elaborates on various upconversion mechanisms in UCNPs, focusing on strategies to boost energy transfer efficiency and prolong luminescence. Subsequently, an in-depth discussion of the various materials that can enhance the efficiency of UCNPs and expand their functionality is provided. Furthermore, a wide range of UCNP-based optoelectronic devices is explored, and multiple emerging applications in UCNP-based neuromorphic computing are highlighted. Finally, the existing challenges and potential solutions involved in developing practical UCNPs optoelectronic devices are considered, as well as an outlook on the future of UCNPs in advanced technologies is provided.

1. Introduction

Optoelectronic devices are fundamental to modern technology, playing a pivotal role in various fields, including information communication,[1,2] environmental monitoring,[3] display technology,[4] storage,[5–7] energy,[8] healthcare,[9] and even quantum information processing.[10] Advances in material composition and device structures have driven remarkable progress in the field of optoelectronics.[11,12] Notably, near-infrared (NIR) responsive optoelectronic devices have garnered substantial scientific interest and potential due to the unique advantages of NIR light, including strong penetration ability, high signal-to-noise ratio, and low optical loss.[13,14] These properties make them particularly well-suited for specialized scenarios such as remote sensing,[15] satellite communications,[16] military encryption,[17] night vision,[18] wearable health monitoring,[19] biomedical imaging, quantum communication,[20] and multilevel data storage.[21] Nevertheless,

S. Geng, H. Li, Z. Lv, Y. Zhai, Y. Luo
College of Electronics and Information Engineering
Shenzhen University
Shenzhen 518060, P. R. China
E-mail: zhaiyb@szu.edu.cn

S. Geng, H. Li, S.-T. Han
Department of Applied Biology and Chemical Technology and Research Institute for Smart Energy
The Hong Kong Polytechnic University
Kowloon, Hong Kong 999077, P. R. China
E-mail: suting.han@polyu.edu.hk

The ORCID identification number(s) for the author(s) of this article can be found under https://doi.org/10.1002/adma.202419678

DOI: 10.1002/adma.202419678

B. Tian
Key Laboratory of Polar Materials and Devices
Ministry of Education
Department of Electronics
East China Normal University
Shanghai 200241, P. R. China

B. Tian
Shanghai Center of Brain-inspired Intelligent Materials and Devices
Shanghai 200241, P. R. China

B. Tian
Chongqing Key Laboratory of Precision Optics
Chongqing Institute of East China Normal University
Chongqing 401120, P. R. China

Y. Zhou
Institute for Advanced Study
Shenzhen University
Shenzhen 518060, P. R. China

conventional NIR optoelectronic devices face challenges in efficiently converting low-energy NIR photons into electrical signals.[22] Under such circumstances, narrow-bandgap semiconductors, such as PbS quantum dots (QDs) and black phosphorus nanosheets, have been explored to address these challenges.[23,24] Although these materials show certain potential, they also face inevitable limitations, including environmental instability, the use of toxic elements,[25] and insufficient photon conversion efficiency, which hinder their further application in next-generation optoelectronic devices. Therefore, developing novel strategies to achieve efficient NIR responsive optoelectronic applications is urgently required.

One promising solution to the aforementioned challenges lies in photon upconversion technology by upconversion nanoparticles (UCNPs). Upconversion luminescence (UCL) is a typical nonlinear anti-Stokes photoluminescence process, where two or more low-energy photons are sequentially absorbed, followed by the radiation transition resulting in the high-energy photon emission.[26,27] This distinctive capability enables UCNPs to efficiently convert NIR light into visible (vis) or ultraviolet (UV) emissions, thereby extending the responsive wavelength range of optoelectronic devices and unlocking features beyond the reach of traditional materials. UCNPs generally consist of a host matrix and specific dopants. Among these, lanthanide ions (Ln^{3+}) doped UCNPs, characterized by their rich 4f orbital energy level,[28] facilitate multistage excitation by absorbing multiple NIR photons, thereby improving the UCL efficiency. Moreover, rare-earth ions, known for their long excited-state lifetimes and stable optical performance, contributed to minimizing energy losses and enhancing emission intensity.[29,30] These intrinsic properties make UCNPs particularly attractive for optoelectronic applications, where efficient photon conversion and precise spectral control are crucial for device performance. Recent advances in nanoscience and nanotechnology have considerably deepened the understanding of UCNPs mechanisms, leading to notable progress in fields such as NIR responsive photodetector,[31,32] three-terminal photonic flash memory,[33–35] and two-terminal photonic memristor.[36]

The upconversion process in UCNPs commonly involves three mechanisms: energy transfer upconversion (ETU), photon avalanche (PA), and energy migration upconversion (EMU).[37] The ETU is the most widely employed mechanism, involving sequential energy transfer between sensitizer and activator ions.[28,38] Yb^{3+} are typically used as sensitizers to absorb NIR photons and transfer energy to activator ions, such as Er^{3+}, Tm^{3+}, or Ho^{3+}, resulting in vis or UV emission. Although Ln^{3+} doped UCNPs offer an effective approach for NIR detection, they still face some shortcomings such as low upconversion efficiency and a limited emission spectrum range, which hinder their further advancement in cutting-edge applications. Addressing these limitations requires precise control of UCNPs' microscopic properties, including host lattice engineering,[39] high-concentration doping,[27] photonic crystal design,[40] and core–shell nanostructure engineering,[41,42] which could reduce nonradiative losses and optimize energy pathways.

However, significant nonradiative losses and the inherent insulating nature of UCNPs hinder their widespread practical application, particularly in light-modulated memory and neuromorphic devices.[43,44] These factors reduce their efficiency in light-modulated memory and neuromorphic devices, making integration into functional electronic systems challenging. Recent efforts to combine UCNPs with other functional materials, such as semiconductors, polymers and plasmonic nanostructures, have opened new avenues for improving device performance and enabling novel applications that surpass conventional materials.[32,43] For instance, combining UCNPs with plasmonic nanostructures, such as Au or Ag nanoparticles (NPs), and optimizing UCL through plasma-enhanced effect can significantly boost optoelectric performance.[45,46] In addition, the combination of UCNPs with semiconductor materials facilitates energy transfer between UCNPs and semiconductors, thereby improving photon-to-electron conversion efficiency.[36,47,48] These composites have enabled the development of high-performance NIR-responsive photodetectors and optical memory devices. In 2014, our group prepared a NIR modulated transistor by integrating UCNPs with semiconducting polymer to develop wearable optoelectric devices.[49] These advancements underscore immense potential of UCNP-based systems for the development of advanced optoelectronic devices. To fully realize this potential, it is crucial to tailor interface properties and optimize composite material synthesis for ensuring efficient energy transfer. Furthermore, refining integration strategies to enhance compatibility with various device architectures and operational environments also deserves attention. Progress in these points will unlock the full potential of UCNPs composites, driving the development for the next generation of smart, multifunctional optoelectronic devices.[34,50]

This review provides a comprehensive overview of recent advancements in UCNP-based optoelectronic devices, focusing on strategies to improve performance and broaden application scenarios (as shown in **Figure 1**). We firstly discuss diverse strategies for improving energy transfer efficiency and luminescence stability, such as dopant concentration optimization and advanced core–shell engineering. Besides, to solve the limitations of high nonradiative loss and inherent insulation properties for UCNPs alone, we review various UCNP-based composites which can enhance the efficiency of UCNPs and expand their functionality. Moreover, we explore a wide range of UCNP-based optoelectronic devices, including photodetectors, three-terminal photonic flash memory, and two-terminal photonic memristors, underscoring the significant progress in harnessing UCNPs' unique properties for diverse applications. We also examine the emerging roles of UCNPs in neuromorphic computing, including convolutional neural networks (CNNs) and reservoir computing (RC). Finally, we propose some targeted solutions to the challenges of integrating UCNPs into practical applications and offer a forward-looking perspective on the role of UCNPs in the future development of advanced optoelectronic technologies.

2. Mechanisms of Upconversion Emission Process in UCNPs

The upconversion emission mechanisms in UCNPs are critical determinants for their emission efficiency, stability, and overall performance, directly influencing their applicability in diverse optoelectronic and photonic applications.[26,51] A thorough understanding of these mechanisms is essential for the rational

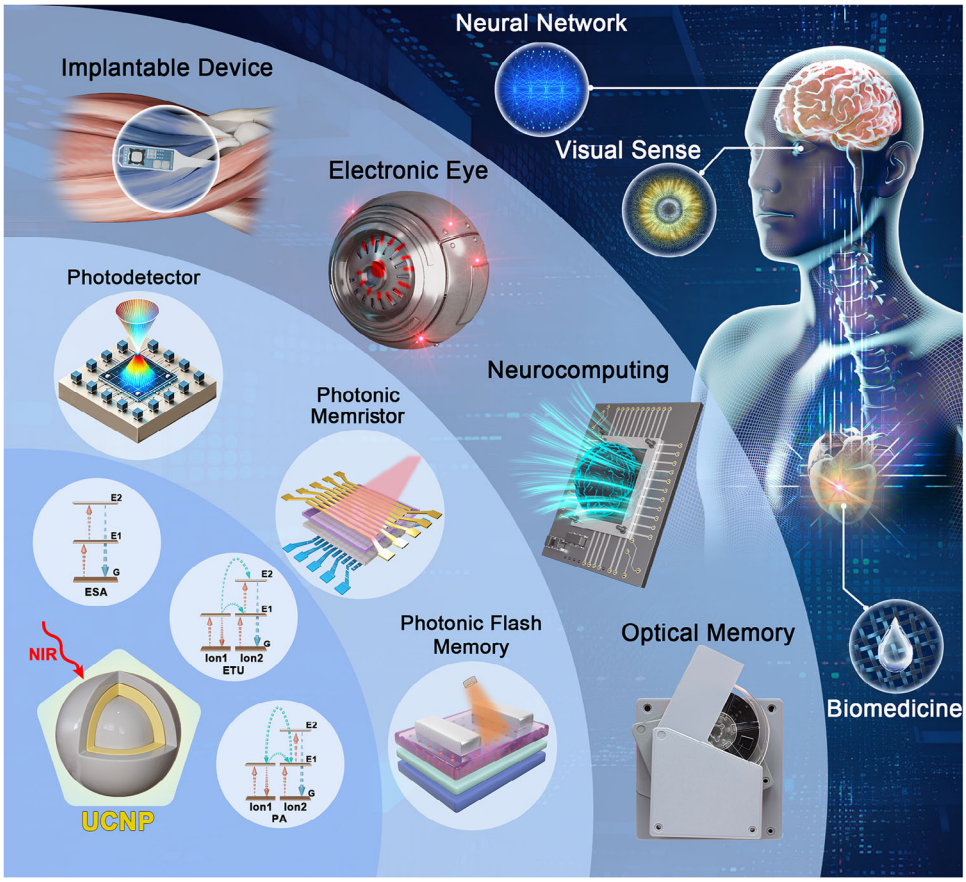

Figure 1. Fundamental mechanisms of UCNPs, and their roles in optoelectronic devices as well as advanced applications.

design and optimization of UCNPs as well as UCNP-based optoelectronic devices, enabling the development of materials that meet the specific requirements of emerging technologies. In this section, we delve into the primary mechanisms responsible for upconversion in UCNPs, focusing on the ETU, PA, and EMU.

2.1. Energy Transfer Upconversion

The ETU is a well-established mechanism in UCNPs that involves a sequential energy transfer process between sensitizer and activator rare-earth ions embedded in a host matrix (**Figure 2a**). Yb^{3+} ions are commonly employed as sensitizers due to their efficient absorption of NIR photons at around 980 nm,[52] while activator ions such as Er^{3+}, Tm^{3+}, or Ho^{3+} are responsible for vis or UV emission. Notably, the excited state absorption (ESA) process involves an activator ion absorbing multiple photons sequentially to reach higher energy states, contributing to enhanced upconversion emission in certain systems.[53] The ESA may coexist with the ETU to increase overall emission intensity. However, compared to the ETU, the ESA typically requires higher excitation power, which limits its efficiency. In addition, the ESA is prone to inducing increased nonradiative losses, potentially further reducing the overall upconversion performance.

The efficiency of ETU is governed by several key factors, including the host matrix's crystal field environment, the ions concentration, and the sensitizer-to-activator ion ratio.[54–56] Selecting host materials with low phonon energies is crucial for minimizing nonradiative decay by reducing vibrational coupling. $NaYF_4$, particularly in its β-phase (hexagonal phase), is highly favorable due to its superior upconversion efficiency.[57] Chen et al. utilized hexagonal-phase β-$NaYF_4$ as the core matrix to examine the relationship between the active domain size (i.e., intermediate shell thickness) and the ETU efficiency.[39] From the absorption spectrum in the range from 300 to 700 nm (Figure 2b), it can be observed that with the increase in the thickness of the intermediate shell doped with Yb/Tm, both the absorbance and the UCL intensity are enhanced. The upconversion quantum yields (UCQY) of UCNPs smaller than 50 nm reached 13.0 ± 1.3%, approximately four times greater than that of conventional micrometer-sized bulk crystals, as shown in Figure 2c. Meanwhile, the measured UCQY rises as the value of shell thickness increases, with the enhancement being particularly pronounced at higher Yb^{3+} concentrations. Benefiting from a relatively high UCQY, these small-sized UCNPs achieve brightness comparable to that of highly efficient single-photon fluorophores, such as semiconductor QDs.

In addition to the conventional $NaYF_4$ host matrix, recent advancements have led to the development of various novel low-phonon-energy host materials, such as sulfide-based systems and double perovskite systems, aimed at further enhancing the energy transfer efficiency. Tian et al. designed a

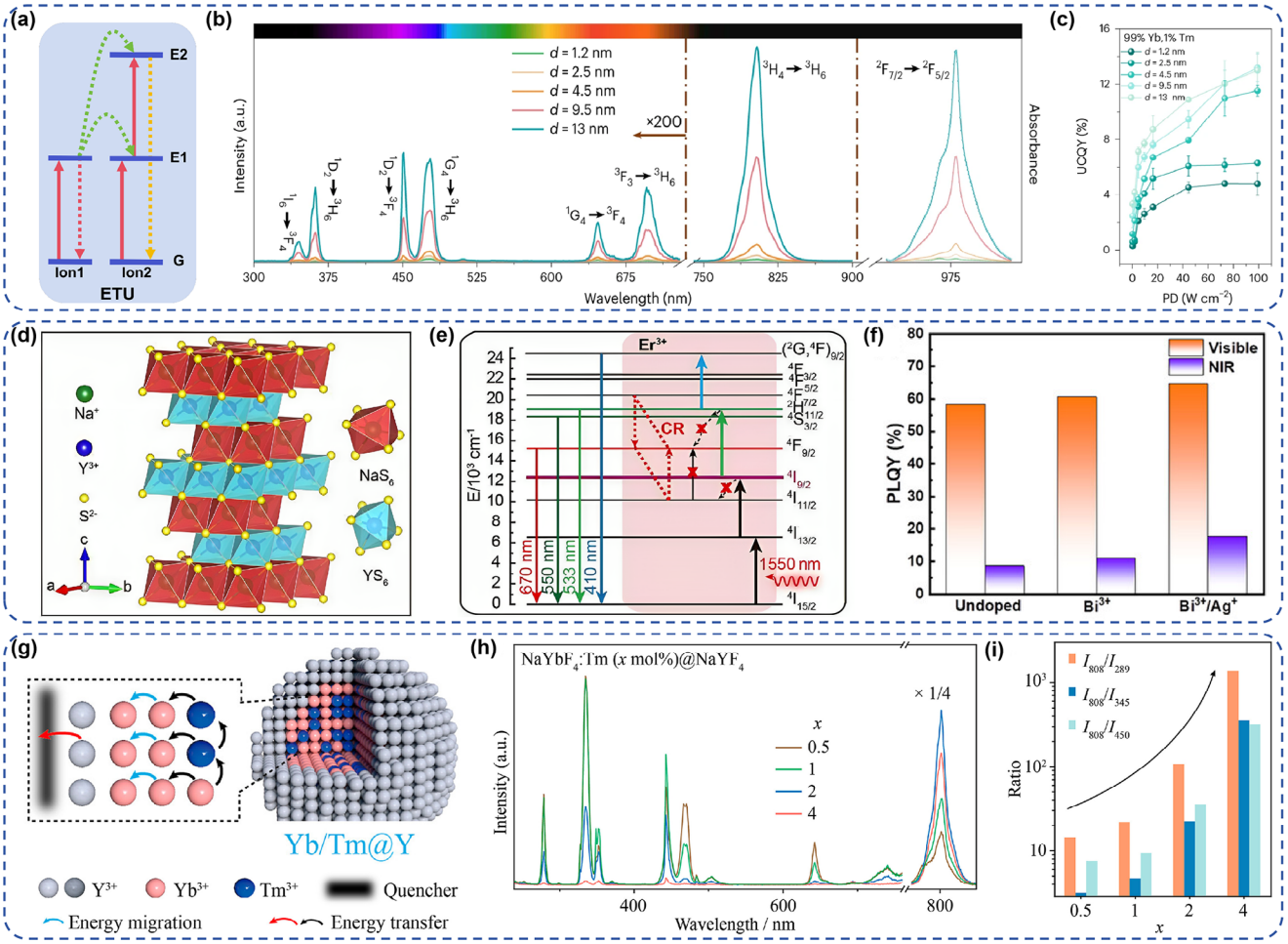

Figure 2. a) Schematic illustration of the ETU mechanism. b) UCL and absorbance spectra of $NaYF_4$@$NaYF_4$:Yb/Tm@$NaYF_4$ core–shell–shell nanoparticles with different shell thicknesses. c) UCQY curves plotted against power density for different shell thicknesses. d) Crystal structure diagram of the ternary sulfide $NaYS_2$. e) Schematic diagram of upconversion mechanism of $NaYS_2$:Er^{3+} crystal under 1550 nm excitation. f) PLQY of Cs_2NaHCl_6 under different doping conditions. g) Schematic depiction of the energy transfer from the emitting core to surface quenchers in Yb/Tm@Y UCNPs. h) UCL spectra of $NaYbF_4$:Tm@$NaYF_4$ core–shell UCNPs with varying doping concentrations under 980 nm excitation. i) The ratio of integrated emission intensity at ≈808 nm relative to those at ≈289, ≈345, and ≈450 nm. b,c) Reproduced with permission.[39] Copyright 2024, Springer Nature. d,e) Reproduced with permission.[58] Copyright 2023, Elsevier. f) Reproduced with permission.[59] Copyright 2023, Wiley. g–i) Adapted with permission.[62] Copyright 2024, Elsevier.

ternary sulfide $NaYS_2$ phosphor doped with Er^{3+} (Figure 2d).[58] The UCL efficiency and brightness reached twice that of commercial β-$NaYF_4$:Yb^{3+}/Er^{3+} phosphors under 980 nm excitation. This significant UCL enhancement can be attributed to the low phonon energy (279 cm^{-1}) of the $NaYS_2$ host matrix and its highly asymmetric trigonal crystal structure, which also mitigates the quenching effect caused by the S^{2-}→Yb^{3+} charge transfer state (Figure 2e). Besides, a holmium-based double perovskite of $Cs_2NaHoCl_6$ was reported, which achieves efficient red NIR emission with a large unit cell and low phonon energy.[59] By doping Bi^{3+} and Ag^+ at the crystal sites, the photoluminescence quantum yield (PLQY) under 450 nm excitation was significantly enhanced to 82.3% (Figure 2f), which can be attributed to the improved crystal field environment that alleviates the parity-forbidden rule and suppresses nonradiative recombination losses. These advancements highlight the critical role of tailored structural engineering and host matrix strategies in exploring photophysical properties.

Regarding doping concentration, although incorporating multiple ions can enhance the sensitization process of UCNPs, placing the ions too close (higher Ln^{3+} doping) can increase nonradiative losses, such as cross-relaxation or quenching, due to excessive energy overlap, ultimately reducing overall emission efficiency. Therefore, developing some methods to achieve high photon quantum yield while increasing doping concentration has become the current research focus. Recently, advancements in nanoparticle research have driven the creation of diverse approaches to mitigate energy loss at heavy doping.[60,61] In a study conducted by Xie et al., a $NaYbF_4$:Tm@$NaYF_4$ core–shell structure was proposed, as shown in Figure 2g.[62] The introduction of a thick inert shell effectively minimized excitation energy dissipation while enhancing absorption, thereby ensuring high energy transfer efficiency. As depicted in Figure 2h, the UCL spectra

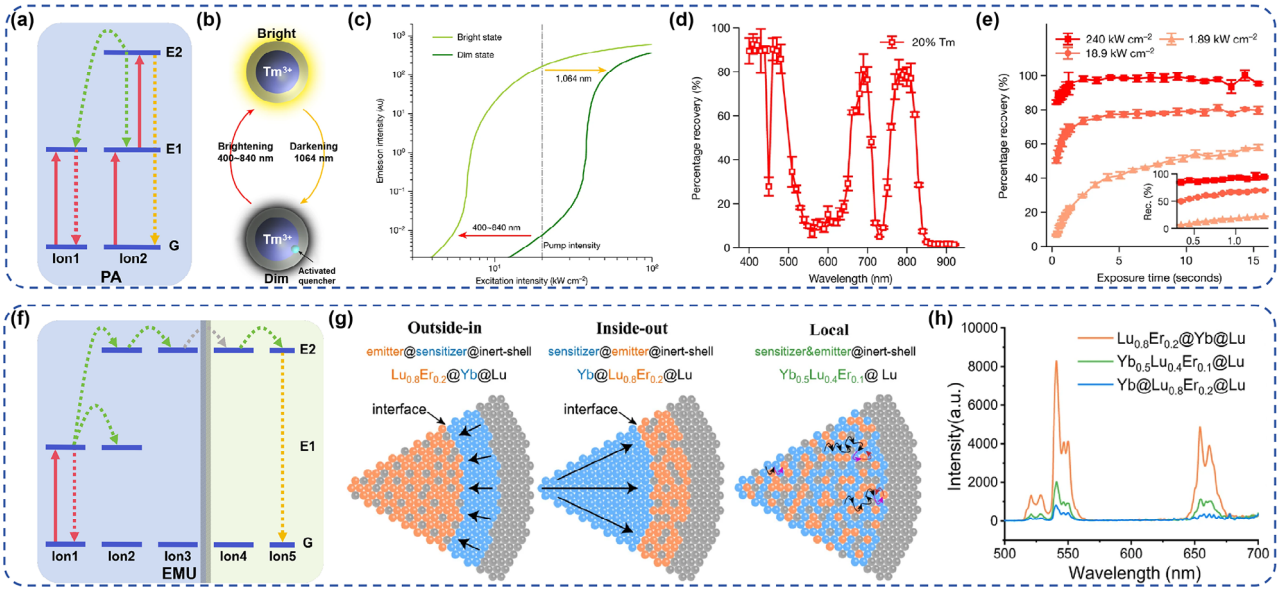

Figure 3. a) Schematic illustration of the PA mechanism. b) Schematic illustration of the fully reversible NIR photoswitching behavior of ANPs. The emission undergoes photodarkening upon exposure to 1064 nm light, while photobrightening is achieved using light in the 400–840 nm range. c) Fitting results of emission intensity versus excitation intensity curves based on differential rate equations, illustrating distinct "bright" and "dim" states under varying excitation conditions. Recovery of photobrightening in a photo-darkened 20% Tm^{3+} core–shell ANP ensemble film sample, analyzed based on d) irradiation wavelength and e) exposure time. f) Schematic illustration of the EMU mechanism. g) Schematic representation of outside-in, inside-out, and local energy transfer configurations. The straight black arrows indicate the dominant energy migration pathway. Er^{3+} are shown as orange spheres, Yb^{3+} as blue spheres, and Lu^{3+} as gray spheres. h) UCL spectra of the UCNPs with core–shell structure under a 980 nm laser (7.3 W cm^{-2}). b–e) Adapted with permission.[69] Copyright 2023, Springer Nature. g,h) Reproduced under the terms of the CC-BY Creative Commons Attribution 4.0 International license (https://creativecommons.org/licenses/by/4.0).[76] Copyright 2022, The Authors, published by Springer Nature.

demonstrate that the individual Tm^{3+} emissions from the core–shell nanoparticles exhibit distinct variations as the doping concentration (*x*%) increases. Furthermore, for core–shell UCNPs with high doping concentrations, the NIR emission becomes increasingly dominant (Figure 2i), and the overall UCL intensity remains largely unchanged. This work provides general design principles to overcome the limitations of traditional heavily doping and to develop UCNPs with high luminous intensity capable of meeting the demands of diverse applications. As a result, incorporating a heavily doping of Ln^{3+} in core–shell structured UCNPs has emerged as a feasible approach to enhance photon upconversion emission intensity.[63]

Overall, the ETU plays a pivotal role in enabling efficient, stable, and high-intensity UCL across diverse excitation regimes. Its high energy transfer efficiency at relatively low excitation power densities, along with the flexibility in precisely tailoring dopant ion concentrations and host matrix environments, underscores its significance in advancing optoelectronic and photonic technologies.[29,64] In current UCNP-based optoelectronic devices, the ETU process is ubiquitously integrated as a core mechanism to achieve tunable multicolor emission and enhanced quantum yields. Furthermore, the ETU serves as the foundational mechanism that supports and enhances various synergistic upconversion processes, such as PA and EMU.[41,50,65] These additional mechanisms build upon the efficient energy transfer provided by the ETU, allowing for further improvements in upconversion performance and enabling the customization of luminescence properties to meet specific requirements optoelectronic device.

2.2. Photon Avalanche

Beyond the well-established ETU process, several other upconversion mechanisms exist that rely on the synergistic interaction of multiple dopant ions to enhance the overall efficiency of UCNPs. Each of these mechanisms possesses unique features that contribute to improving different aspects of upconversion performance. The PA is a highly nonlinear mechanism characterized by an initial weak photon absorption that triggers a positive feedback loop of energy transfer, leading to rapid and significant amplification of upconversion emission.[66,67] The schematic diagram of the PA mechanism is shown in **Figure** 3a. This mechanism requires a threshold excitation power, beyond which the emission intensity increases dramatically, making it particularly suitable for applications that demand on-off switching behaviors or high-intensity emission outputs, such as optical sensors and memory devices.[68] Figure 3b shows a switching process of light-controlled switch based on Tm^{3+} doped avalanching nanoparticles (ANPs).[69] The mechanism of such optical switch involves modulating the threshold intensity of PA using NIR-I (700–900 nm) and NIR-II (1000–1700 nm). Impressively, after over 1000 repeated optical switching cycles, the emission intensity of ANPs in this light-controlled switch exhibited negligible attenuation (Figure 3c), demonstrating excellent stability and durability. This stability makes ANPs a promising candidate for 2D/3D multicolor optical information storage. Figure 3d confirms the dependence of luminescence recovery on the illumination wavelength, with peaks at 800 and 700 nm directly corresponding to the Tm^{3+} $^3H_4$ and $^3F_{2,3}$ transitions, while the peak at 530 nm

is attributed to color centers. Moreover, boosting the exposure duration or irradiation intensity could further promotes photobrightening. When exposed to 700 nm light, almost full luminescence recovery can be attained within seconds (Figure 3e). This PA-based devices could achieve precise multicolor emission control, enabling high-density, multidimensional optical storage with remarkable durability.[70] In addition, by optimizing dopant concentration and host materials, the excitation threshold can be further reduced, enhancing the energy efficiency of PA-based devices and adaptability to diverse practical applications.[71]

2.3. Energy Migration Upconversion

The PA mechanism involves the direct interaction of photoexcited states with target sites, while the EMU mechanism relies on cooperative energy migration between multiple excited states.[72] As shown in Figure 3f, the EMU occurs when the excitation energy migrates through a network of sensitizer ions before reaching an activator ion capable of emitting a photon. This mechanism is particularly effective in multilayer core–shell UCNPs, where a sensitizer-rich core allows efficient energy migration, which is then transferred to an activator-doped shell for emission.[73–75] The EMU supports effective long-range energy migration, enhancing emission uniformity and boosting overall efficiency. Liu et al. designed three types of core–shell structured UCNPs (Figure 3g), with different energy migration directions, to investigate the factors influencing energy loss during the EMU process.[76] As illustrated in Figure 3h, the luminescence spectra indicates three structures' UCL emission. The peaks at 521, 541, and 654 nm correspond to the radiative transitions of Er^{3+} from the $^4I_{11/2}$, $^4S_{3/2}$, and $^4F_{9/2}$ states, respectively. Notably, the "outside-in" structure demonstrates the strongest UCL, suggesting that interfacial energy transfer plays a crucial role in enhancing UCL. This designed structure leverages directional energy migration through topological optimization, providing an innovative strategy to enhance EMU efficiency. This approach not only increases single-particle brightness but also minimizes back-transfer energy losses at the interface. Regulating the energy migration pathways through topological structure breaks away from the traditional design paradigm of upconversion materials, offering a new perspective for developing high-efficient upconversion systems.

Overall, the interplay between these synergistic upconversion mechanisms allows for precise tuning of UCNPs' emission characteristics.[77,26] By carefully optimizing dopant concentrations, selecting appropriate host matrices, and designing core–shell structures, precise control over the upconversion efficiency and emission spectra can be achieved.[78]

3. Hybrid Materials Based Upconversion System

In the previous chapter, we have explored the fundamental mechanisms of UCNPs and discussed various strategies to enhance the energy transfer efficiency. While UCNPs exhibit great potential in a wide range of applications, their integration into optoelectronic devices, particularly memory-type devices, still faces significant challenges due to their substantial nonradiative losses and inherent insulating nature. These limitations make them less effective in advanced applications like high-sensitivity photodetectors and neuromorphic devices.

Many studies have focused on integrating UCNPs with other functional materials to form composites that not only improve UCL intensity but also expand their application scope, overcoming their inherent limitations and fulfilling the specific requirements of emerging optoelectronic applications. In this section, we classify UCNP-based composites into two main categories: (1) those that enhance the absorption capability of UCNPs and improve UCL intensity, such as nanometallic particles and organic dyes,[45,79] and (2) those that broaden the absorption spectrum and expand UCL functionality, such as QDs, 2D materials, and metal–organic frameworks (MOFs).[48,80–82]

3.1. Materials for Enhancing UCL Intensity

The intensity of UCL is a critical factor in enhancing the performance of UCNP-based optoelectronic devices, as it directly affects their efficiency, sensitivity, and functionality. However, UCNPs are inherently limited by low photon absorption efficiency and significant nonradiative losses, which restrict their effectiveness across various applications. Incorporating certain materials such as metallic NPs or organic dyes into UCNPs can enhance the NIR absorption of UCNPs, optimize energy upconversion processes, and reduce nonradiative decay, thereby boosting overall UCL efficiency.

Metallic NPs such as Au, Ag, or Cu NPs are among the most effective materials for improving UCNPs performance through plasmon-enhanced upconversion (PEU).[83] In the PEU process, the energy from the metallic NPs is transferred to the UCNPs via nonradiative coupling, which increases the photon absorption capability in the NIR region. Furthermore, these plasmonic nanostructures are known for their ability to concentrate light through localized surface plasmon resonances (LSPR), which significantly increase the electromagnetic field near the nanoparticles surface when illuminated by incident light (**Figure 4a**).[45] This local field enhancement results in a higher excitation rate of UCNPs. For instance, the LSPR of Au and Ag NPs can strongly interact with the UCNPs, enhancing their light-harvesting capacity and significantly boosting the upconversion emission intensity. In addition, the localized electromagnetic fields generated by plasmonic NPs can suppress the nonradiative decay pathways, which further contributes to the improvement of UCL efficiency. Therefore, this interaction not only enhances the photon absorption but also reduces nonradiative losses by facilitating the efficient transfer of excitation energy from metallic NPs to the UCNPs.

In most metal–UCNPs composites, metallic NPs are typically attached to the surface of UCNPs. Therefore, the size of the metallic NPs are essential contributors to the luminescence efficiency of UCNPs, as it indirectly influences the thickness of the metal shell on the UCNPs surface. Díaz et al. investigated how the size of the Au NPs affects plasmonic excitation mechanisms.[84] Larger Au-NPs strengthen the emission intensity through PEU, but the peak of LSPR gradually shifts away from the UCNPs emission region (Figure 4b). While small-sized Au-NPs cannot effectively generate

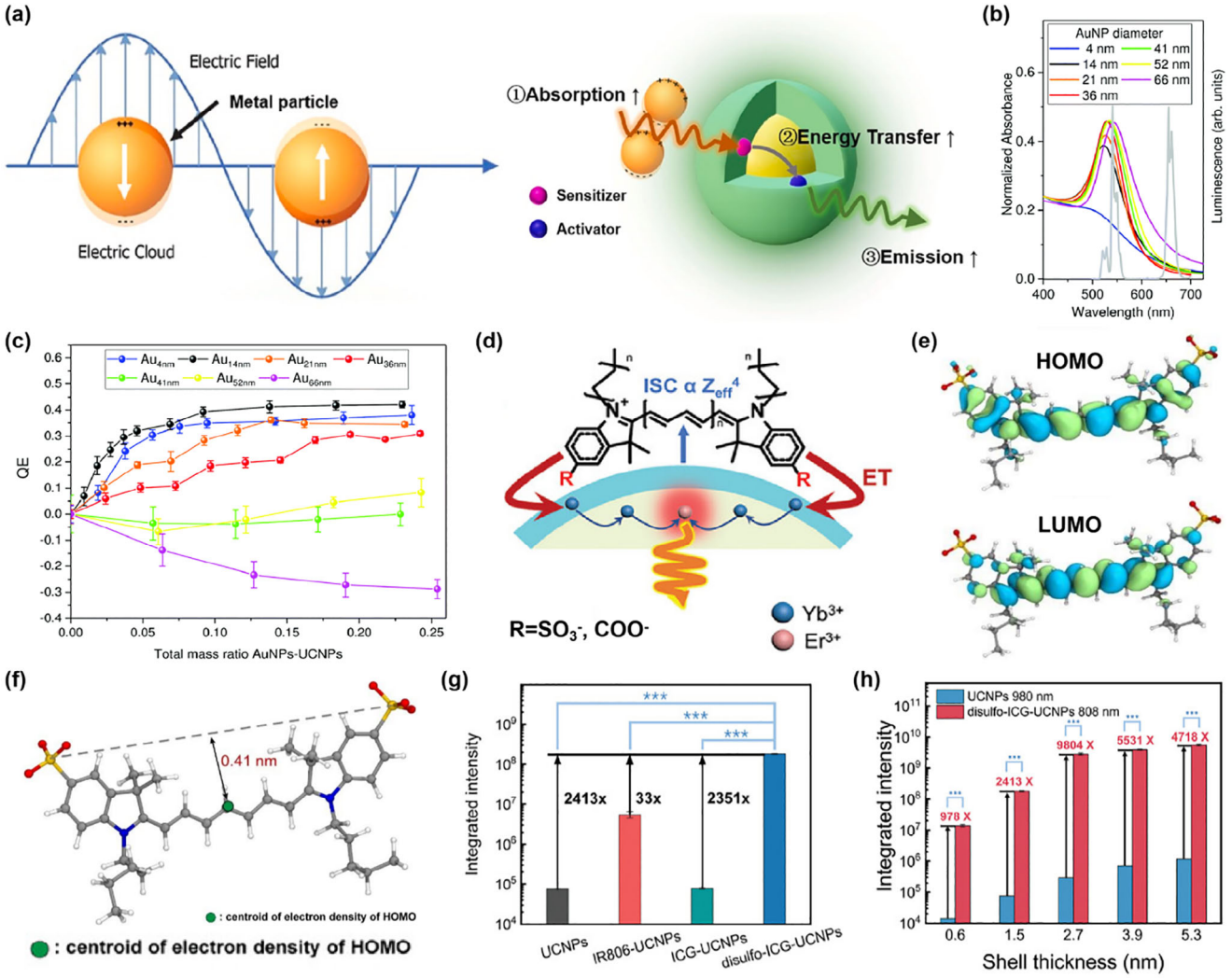

Figure 4. a) The principle of LSPR and a schematic illustration of the upconversion process in UCNPs combined with metallic NPs. b) Emission spectra of UCNPs ethanol dispersions combined with Au-NPs of different sizes. c) UCL quenching efficiency of UCNPs combined with different sizes and ratios of Au-NPs. d) Chemical structure diagram of the dye and the schematic illustration of the energy transfer mechanism. e) The frontier molecular orbitals of cyanine dyes, incorporating sulfonate groups on their aromatic components, which consist of the highest occupied molecular orbital (HOMO) and the lowest unoccupied molecular orbital (LUMO). f) The optimized geometric configuration of cyanine dyes coordinated with Yb^{3+}, where the distance between the fluorescent core and the Yb^{3+} on the UCNPs surface is 0.41 nm. g) Integrated intensity of pure UCNPs and UCNPs combined with various dyes under excitation by 980 and 808 nm lasers. h) Integrated intensity of pure UCNPs and disulfo-ICG modified UCNPs with different shell thicknesses under excitation by 980 and 808 nm lasers. a) Reproduced with permission.[45] Copyright 2023, Elsevier. b,c) Reproduced with permission.[84] Copyright 2019, Royal Society of Chemistry. d–h) Reproduced with permission.[89] Copyright 2023, Wiley.

plasmon-resonance-enhanced UCL and are prone to quenching. Only in an intermediate size range (41–52 nm), two plasmon-induced phenomena roughly compensate each other, resulting in a quenching efficiency (QE) close to zero (Figure 4c). Furthermore, the combination of UCNPs with metallic NPs has shown exceptional performance in various optoelectronic applications, including photodetectors and biosensors, significantly enhancing sensitivity and lowering detection limits. Meanwhile, these composites have also demonstrated improved stability and reproducibility in NIR based devices, making them ideal for advanced imaging sensors and systems. Furthermore, the versatility of metallic NPs allows for tuning the excitation wavelength and emission intensity in UCNPs, making these composites highly adaptable for different applications.

Another effective approach to enhance UCL intensity is to form UCNPs/organic dyes composites, in which organic dyes act as sensitizers to promote energy transfer via Förster resonance energy transfer (FRET).[85] Organic dyes absorb low-power pump light and transfer the energy nonradiatively to the sensitizer ions of UCNPs (such as Yb^{3+} or Er^{3+}), potentially enhancing upconversion luminescence and energy conversion efficiency, depending on the energy transfer efficiency and system design. Dyes such as rhodamine B,[86] coumarin,[87] and Nile blue[88] have been successfully integrated with UCNPs to boost their efficiency in medical diagnostics, luminescent sensors, and solar cells. These

dyes can also tune the emission spectra of UCNPs, providing a way to tailor the upconverted light for specific applications. Liu et al. reported a specially designed NIR dye, disulfo-indocyanine green (disulfo-ICG), which enhances the emission intensity of UCNPs.[89] The chemical structure of dye and energy transfer mechanism are presented in Figure 4d. Cyanine molecules are anchored to the surface of UCNPs via coordination bonds formed between Ln^{3+} and carboxylate or sulfonate functional groups, enhancing the functional integration of the materials. Notably, alkyl chains increase the distance between the fluorescent core and the UCNPs surface, which in turn reduces the energy transfer efficiency. Therefore, this work modifies the coordinating groups on the conjugated structure to reduce the distance between the fluorescent core and Ln^{3+}, thus enhancing the heavy-atom effect of the Ln^{3+} on the dye (Figure 4e,f). Two sulfonate-modified disulfo-ICG on the aromatic portion produces an exceptionally strong dye-sensitized UCL emission (Figure 4g), which is 2413 times higher than the pure UCNPs emission. In addition, the upconversion emission enhanced by dye sensitization is also influenced by the thickness of the UCNPs active shell, as presented in Figure 4h. As the thickness of the outer shell increases, the dye-sensitization enhancement factor first rises and then gradually declines, with the maximum enhancement observed at 2.7 nm. This work broadens the scope of NIR upconversion sensitizing dyes and introduces a new approach to modifying dye ligands, providing valuable insights into the development of efficient upconversion composite systems. Furthermore, organic dyes, known for their high molar extinction coefficients and photochemical stability, are ideal for improving the quantum yield of UCNPs. By using dyes that can strongly absorb in the NIR region and efficiently transfer energy to UCNPs, it is possible to achieve higher UCQY and increase the luminescence intensity, making these composites highly efficient for low-power optical applications.[90–93]

3.2. Materials for Expanding UCL Functionality

While improving the intensity of UCL is a crucial step, integrating them with other materials to expand their functionality is equally important for establishing a robust foundation for advanced NIR optoelectronic devices. Combining UCNPs with materials such as QDs, 2D materials, and MOFs can introduce some novel properties that UCNPs alone cannot achieve. These composites improve energy transfer, facilitate efficient photon–electron conversion, and provide functionalities like high mechanical flexibility and improved charge transport. Such synergies between these materials have further propelled the development of multifunctional optoelectronic devices.

One of the most common materials used to augment the functionality of UCNPs is QDs, known for their high quantum yield and vibrant fluorescence across a wide spectrum. Among QDs, perovskite have gained prominence due to their tunable physical properties and cost-effective synthesis, making them ideal for applications in photodetectors, and optical sensors. Since UCNPs generally limited by their narrow absorption spectrum and low energy conversion efficiency, integrating them with perovskite QDs can obtain great benefits. The key advantage of combining UCNPs with perovskite QDs lies in their complementary energy levels for efficient energy transfer.[43] UCNPs transfer energy to perovskite QDs through their NIR UCL properties, with the perovskite QDs utilizing this energy for light emission. This combination improves optical responses and luminescence efficiency. Furthermore, the wide tunability of perovskite QDs allows for tailoring emission spectra from the UCNPs, making these composites highly versatile for a variety of applications.[94] Van et al. reported an effective strategy for NIR pumping of $CsPbBr_3$ QDs via energy transfer from $BaYF_5$:Yb/Tm UCNPs.[95] The upconversion mechanism is presented in **Figure 5**a, where the $^5F_3$ level of Ho^{3+} and the $^1D_2$ and $^1G_4$ levels of Tm^{3+} are energetically higher than the conduction band of $CsPbBr_3$ QDs. Furthermore, there is a strong spectrum overlap between the absorption spectrum of the QDs acceptor and the emission spectrum of the UCNPs donor, which enables high transfer efficiency from UCNPs to QDs via photon reabsorption (PR) or FRET. The UCL spectra of UCNPs/QDs composites with different doping ratios under 975 nm excitation (Figure 5b) confirm this. Figure 5c illustrates the variation in integrated UCL intensities of different components from Figure 5b as the UCNPs/QDs ratio changes. With the increase in perovskite QDs concentration, the overall emission intensity of the $CsPbBr_3$ band shows a roughly linear increase. Furthermore, at a 1:0.125 ratio, the integrated intensity of the Tm^{3+} $^1G_4$–$^3H_6$ transition decrease by ≈98%, and it completely vanish in the sample with the maximum acceptor concentration, indicating an energy transfer efficiency of nearly 100% from $BaYF_5$:Yb/Tm to $CsPbBr_3$. These composites also benefit from the high stability of perovskite QDs, and the synergy between UCNPs and perovskite QDs improves both the stability and quantum yield of the resulting devices.[96] The UCNPs/QDs composites have shown great promise in solar energy harvesting, where they can be used in photodetectors devices.

Recent years, 2D materials have gained attention for their high surface area and remarkable electronic properties. These materials also exhibit tunable optical, electrical, and mechanical characteristics, making them ideal for integration with UCNPs. This combination addresses inherent limitations of UCNPs, including low charge transport efficiency and poor photon–electron conversion.[48,97] Among them, MoS_2 has gained attention due to its high electronic conductivity and direct bandgap in monolayer form, which allows for effective energy transfer and charge separation in optoelectronic devices. By integrating MoS_2 with UCNPs, the charge transfer efficiency between the UCNPs and MoS_2 is significantly improved, resulting in enhanced photodetectors and sensor performance.[36] In addition, these composites exhibit photobleaching resistance, minimal background fluorescence interference, excellent biocompatibility, and high photothermal conversion efficiency. Furthermore, the combination of UCNPs with MoS_2 also enhances the material's optical absorption in NIR wavelength, complementing UCNPs' capability to convert NIR into visible light, which makes the composites highly suitable for high-performance imaging, sensing, and energy harvesting applications. Huang et al. designed a hollow MoS_2 architectures on the $NaYF_4$:Yb/Er microtubes, which facilitated efficient resonance energy transfer and significantly enhanced the UCNPs' response.[98] The transmission electron microscope (TEM) and high-resolution TEM images of the MoS_2 thin layers and the $NaYF_4$:Yb/Er coating are shown in Figure 5d, where MoS_2 is evenly distributed on the microtubes surface.

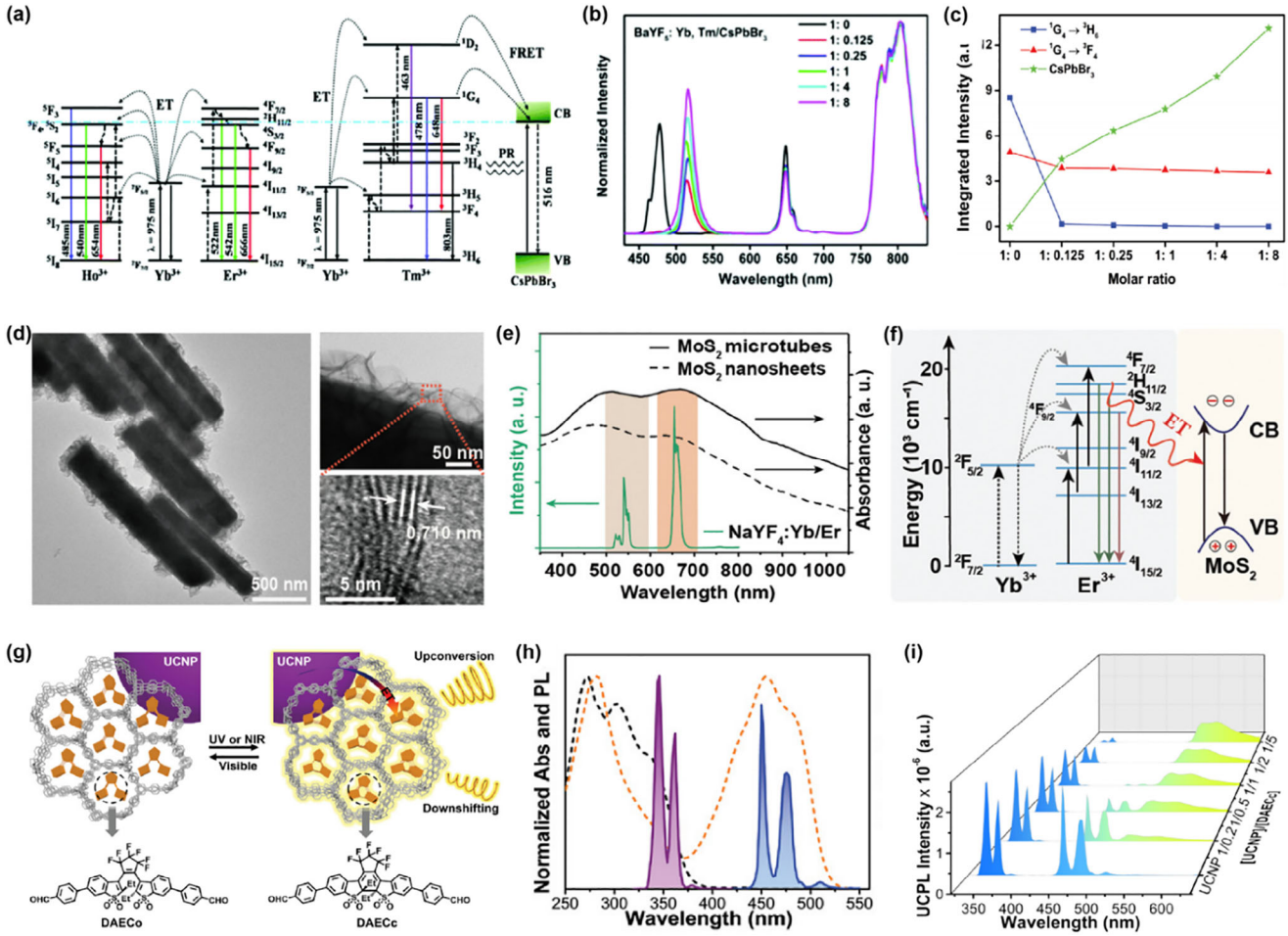

Figure 5. a) Schematic energy level diagram of the upconversion process and energy transfer mechanism in $BaYF_5$:Yb/Ln-$CsPbBr_3$ composites under 975 nm laser excitation. b) UCL emission spectra of $BaYF_5$:Yb/Tm-$CsPbBr_3$ QDs at different ratios under 975 nm laser excitation. c) Variation in the integrated UCL intensities of the components in (b) as a function of the doping ratio of $BaYF_5$:Yb/Ln-$CsPbBr_3$. d) TEM and HRTEM images of $NaYF_4$:Yb/Er-MoS_2 composite. e) Absorption spectra of MoS_2 microtubes and nanosheets, and UCL spectra of $NaYF_4$:Yb/Er (980 nm laser excitation). f) Diagram illustrating the energy transfer process between $NaYF_4$:Yb/Er and MoS_2 during the upconversion process. g) Schematic diagram of the dual CPL switch for upconversion and DS in UCNPs-MOFs@DAEC activated by optical stimuli. h) The absorption spectra of DAECo (black dashed line) and DAECc (orange dashed line), along with the UCL emission spectra of PVP-modified UCNP-Tm under 980 nm laser excitation. i) Normalized UCL spectra of UCNPs-MOFs@DAEC with varying proportions under 980 nm laser excitation. a–c) Reproduced with permission.[95] Copyright 2019, Royal Society of Chemistry. d–f) Reproduced under the terms of the CC-BY Creative Commons Attribution 4.0 International license (https://creativecommons.org/licenses/by/4.0).[98] Copyright 2020, The Authors, published by Wiley-VCH. g–i) Reproduced with permission.[103] Copyright 2021, Wiley.

The absorption spectrum of MoS_2 and the emission spectrum of $NaYF_4$:Yb/Er (excited at 980 nm) exhibit nearly complete spectral overlap, indicating the efficient nonradiative energy transfer between these two components (Figure 5e). Figure 5f illustrates the energy transfer process during the upconversion process in the composite structure, where the energy from UCL emission is efficiently transferred to the tightly bound MoS_2 thin layers, significantly reducing radiative energy losses and providing a solid performance foundation for subsequent optoelectronic devices. Moreover, the high flexibility and mechanical properties of 2D materials, exemplified by MoS_2, provide significant advantages for the development of wearable optoelectronic devices and flexible photodetectors. This ability to design stretchable or bendable UCNP-based devices makes them highly attractive for bioelectronics and environmental sensing applications, where flexibility is crucial.[99,100]

In addition to 2D material, the UCNPs-MOFs heterostructure demonstrates promising potential in applications such as biosensors and imaging, drug delivery, and photodynamic therapy (PDT).[101] MOFs are a class of materials characterized by their high surface area, tunable porosity, and exceptional chemical and thermal stability. These materials consist of metallic ions or clusters bonded to organic ligands, creating a 3D network structure. The synergy effect between MOFs and UCNPs is primarily attributed to the ability of MOFs to act as both energy donors and structural scaffolds.[92,102] On the one hand, MOFs can absorb low-energy photons, such as those in the NIR range, and transfer this energy to UCNPs through nonradiative

interactions, resulting in efficient upconversion emissions. On the other hand, the porous structure of MOFs facilitates seamless integration with UCNPs, enhancing charge separation and minimizing nonradiative losses. Furthermore, the high surface area and tunable porosity of MOFs, including factors such as pore size, play a crucial role in enhancing light harvesting and charge transport. These structural characteristics, when combined with the high quantum efficiency of UCNPs, not only improve photodetection sensitivity and response speed but also influence the fluorescence lifetime and enhance photon yield by modulating energy transfer dynamics and minimizing nonradiative losses. In short, combining MOFs with UCNPs significantly improves dispersibility, stability, and, most critically, energy transfer efficiency, along with improved charge separation and transport, thereby enhancing the overall performance of UCNP-based optoelectronic devices. Moreover, the incorporation of MOFs into optical storage devices improves both the stability and storage capacity, providing new possibilities for data storage and security applications. Duan et al. reported a dual-switch system demonstrating both upconversion and downshifting (DS) circularly polarized luminescence (CPL) in the solid state was developed by integrating diaryl ethylene derivatives (DAEC) and $NaYF_4$:Yb/Tm UCNPs into chiral MOFs (Figure 5g).[103] The isomers of DAEC can switch between the open-ring form (DAECo) and the luminescent closed-ring form (DAECc), a process that can be triggered by the application of Vis and UV/NIR light. Figure 5h shows the normalized absorption spectra of DAECo and DAECc, along with the UCL emission spectra of UCNPs-Tm. The emissions of UCNPs-Tm at 346 and 362 nm align with the absorption bands of DAECo, while the UV emissions at 450 and 476 nm can be absorbed by DAECc. Thus, the transformation of DAECo to DAECc is attributed to the UV emission from UCNPs-Tm under NIR 980 nm laser excitation. As the DAECc content in the UCNPs-MOFs@DAEC composite increases, the relative UC emission intensity of DAECc gradually rises, while the UCNPs-Tm emission decreases, further demonstrating the high energy transfer efficiency between UCNPs-Tm and DAECc (Figure 5i). By tuning the chemical composition and porous structures of MOFs, it is possible to optimize the energy transfer dynamics and emission properties of UCNPs, thereby improving their efficiency and versatility in various technological fields. These composites are anticipated to serve a pivotal role in the development of next-generation smart devices for applications in light sensing, photodetectors and optical information storage.

Overall, the integration of various composite materials significantly enhances UCNPs' performance, improving the UCL intensity and overcoming limitations such as poor charge transport and high nonradiative losses. In addition to the materials discussed earlier, others like poly(3-hexylthiophene-2,5-diyl) (P3HT) and graphene oxide (GO) can also be combined with UCNPs to further improve their properties.[104,105] P3HT, a conductive polymer, helps to facilitate energy transfer and charge separation, enhancing the efficiency of devices like photodetectors and photoelectronic memory. Meanwhile, GO, a 2D material, improves the charge transport properties and adds flexibility, making UCNPs-GO composites more suitable for wearable and flexible optoelectronic devices. These advanced UCNP-based composites provide a robust foundation for the development of NIR optoelectronic devices, where efficient energy management, high sensitivity, and fast response times are essential for next-generation smart systems.

4. UCNP-Based Optoelectronic Devices

The excellent optical properties of UCNP-based composites significantly enhance signal strength and clarity, making their reliable integration with optoelectronic devices an important topic for diversifying optical device functionalities. For example, the successful integration of UCNPs with CdS semiconductor has produced a high-performance NIR photodetector, which not only improves the photoresponsivity and external quantum efficiency by 14-fold and 140-fold, respectively, but also overcomes the wavelength limitation of traditional CdS based photodetectors.[106] In addition, encapsulating UCNPs within a WO_3 hydrogel matrix with photochromic properties circumvents polarization dependence issues of conventional silicon-based optical switches, effectively reduces energy cross interference, and improves the purity and controllability of optical signals.[107] Furthermore, optoelectronic devices based on UCNPs and P3HT exhibit higher ON/OFF ratios, wider storage windows (6.3%–34%), and longer retention times, enabling the development of a photonic neuromorphic device with multilevel storage and tunable conductivity.[49] These advancements illustrate the potential of synergistic UCNP-based composites for next-generation optoelectronic applications. To clearly illustrate the importance of UCNP-based composites in various optoelectronic device, this section reviews the latest advancements of UCNP-based photodetectors, three-terminal photonic flash memory, and two-terminal photonic memristors. Moreover, we provide a detailed summary of the relationship between materials properties and device performance, offering both theoretical and empirical guidance for the development of high-performance optoelectronic devices.[108,109]

4.1. Photodetector

Photodetectors are devices that convert light signals into electrical signals through the photoelectric effect, making them crucial in fields such as detection and imaging.[110,111] When the energy of photons exceeds the band gap of semiconductor materials, electron–hole pairs are excited, causing changes in current or voltage within the circuit.[112,113] A high-performance photodetector should feature wide spectral range; however, the traditional photodetectors are typically limited to vis[114,115] or UV[116] light and exhibit limited sensitivity to long-wavelength NIR light. Therefore, integrating UCNPs with other functional materials has emerged as a promising strategy for achieving advanced NIR photodetectors.[17,117] In the research process, the key parameters of photodetectors determine their sensitivity, speed, and overall performance, such as response/recovery time, quantum efficiency, and sensitivity. For the response/recovery time, incorporating 2D materials (such as graphene and MoS_2) with UCNPs accelerates the separation of photogenerated electron–hole pairs, significantly enhancing response speed.[118,119] In terms of quantum efficiency, coupling UCNPs with high-absorption

materials (e.g., GaAs) improves quantum efficiency, especially under low-light conditions, resulting in greater photosensitivity and a lower detection limit.[120] For the sensitivity, engineering heterojunctions with larger barriers enhances charge carrier separation, suppresses recombination losses, and extends exciton lifetime, increasing charge collection efficiency and boosting the signal-to-noise ratio in photodetection. To assess material performance, techniques like time-resolved photoluminescence (TRPL) analyze exciton dynamics, such as exciton lifetimes and carrier recombination rates, which are crucial for efficiency and response.[121] The integration of UCNPs with these functionals materials not only extends the detection spectrum but also improves performance, making it particularly advantageous for applications with high NIR sensitivity and responsivity.

The performance of NIR-responsive photodetectors typically depends on the NIR absorption capability, the absolute UCL intensity of the UCNPs, and the film quality of the electron transport layer. As mentioned earlier, one of the most effective approaches to enhance the light absorption capability of UCNPs is through modification with metallic NPs, leveraging the plasmon-enhanced upconversion effect to improve both detection efficiency and response time. This enhancement is mainly related to ETU. In the current photodetectors using UCNPs, the vast majority of researchers choose to use Yb^{3+} as sensitizers, absorbing NIR light and transferring energy to Er^{3+} activators to produce visible or ultraviolet emissions. Park et al. reported high-performance two-terminal photodetector based on ternary nanostructured UCNPs-Au-PB (Prussian Blue) (**Figure 6a,b**).[122] The incorporation of Au NPs induces LSPR, significantly enhancing the single-photon absorption capability of Er^{3+} in the UCNPs and thereby improving light absorption efficiency. In addition, PB, as a broadband absorption material, extends the absorption range across the Vis and NIR regions and facilitates photoinduced charge transfer, increasing the carrier density of the device. The synergistic interaction among these three materials enables this photodetector to exhibit superior cost-effectiveness, exceptional sensitivity, and outstanding responsivity compared to other similar nanocomposite devices. Under irradiation with various wavelengths (432–980 nm) at the same power density (3.184 mW cm^{-2}), the UCNPs-Au-PB based device achieves a photocurrent of 29 μA, nearly ten times greater than the 3.3 μA observed in the original PB-based photodetector (Figure 6c,d). In additional, Ko et al. proposed that energy transfer from UCNPs to Au core–satellite nanoassemblies (CSNA), driven by both radiative and nonradiative modes, significantly facilitates the efficient separation of electron–hole pairs and their effective channeling.[123] By incorporating Au NPs, the NIR absorption of UCNPs are enhanced, and this composite is integrated into indium tin oxide (ITZO) transistors, setting a precedent for the development of NIR imaging sensor systems based on metal oxide semiconductors. This enhancement arises from the energy transfer between UCNPs and Au NPs, which facilitates the effective separation of electron–hole pairs generated within the Au upon the application of drain voltage and directs these charge carriers into the conduction band of the ITZO semiconductor. This mechanism significantly improves the efficiency of the device, allowing for the successful development of a NIR imaging system. Notably, regardless of the shape of the metallic NPs, the plasmon-enhanced upconversion effect can efficiently increase the UCL intensity.

Moreover, combining UCNPs with semiconductors is also an outperform strategy, where UCNPs serve as the light absorbers, while the semiconductor materials act as efficient charge transporters. However, the roughness of the UCNP-based composites directly affects the film formation quality of the electron transport layer, which in turn impacts the performance of the photodetector. Dong et al. designed a three-phase self-assembly method, which differs from simple spin-coating technique, to fabricate large-area, flat, and dense monolayers of Au@Ag nanorods and UCNPs, as shown in the TEM image (Figure 6e).[124] This method can effectively reduce the roughness of the UCNPs layer, thereby enhancing the electron mobility in the $MAPbI_3$ film. Furthermore, the incorporation of Au@Ag nanorods significantly improves the UCL peak compared to pure UCNPs (Figure 6f). Through the combined optimization of these two methods, the response performance of the photodetector can be improved by two orders of magnitude. In addition, Song et al. employed UCNPs/perovskite arrays to construct lateral heterostructured photodetector sensitive to both vis–NIR light (Figure 6g,h).[125] Due to the overlap between the UCL spectrum of UCNPs and the absorption spectrum of the $CsPbI_{2.2}Br_{0.8}$ array, the UCNPs/perovskite heterostructure can respond to both Vis and NIR. Therefore, this device demonstrates excellent light-harvesting ability of vis–NIR light and ultra-higher photocurrent under 980 nm illumination (Figure 6i). These studies demonstrate that UCNPs not only enhance the intrinsic optical sensitivity of other materials, but also broaden the response range into the infrared spectrum, significantly expanding the potential applications of NIR photodetectors.

4.2. Optoelectronic Memory Device

With the rapid growth of data volume, traditional memory technologies are struggling to meet the increasing demand for high density and low power consumption. Photonics facilitate data storage and processing through optical methods, providing exceptional bandwidth and speed.[126] Photonic memory systems replace conventional electrical wiring with on-chip optical interconnections to connect memory units and central processing units (CPUs).[127] This approach addresses the von Neumann bottleneck by lowering power consumption and improving data communication speed. These photonic memories can be directly integrated into processor chips, thereby enhancing the efficiency of optical data transfer. However, as Moore's law becomes increasingly obsolete, further miniaturization to incorporate more memory cells is hindered by the complexities of fabrication and photolithography. An alternative strategy involves developing multilevel memory cells with high storage density, shifting the focus to achieving distinct and stable states. In photonic memories, light signals act as an additional terminal in memristor devices, ensuring a wide memory window and significant variation margin across multiple storage levels. UCNPs provide new possibilities for optoelectronic memory devices that utilize NIR optical signals for regulation and computation, offering promising prospects for advanced brain–computer interfaces and biological neural network simulations in the future.

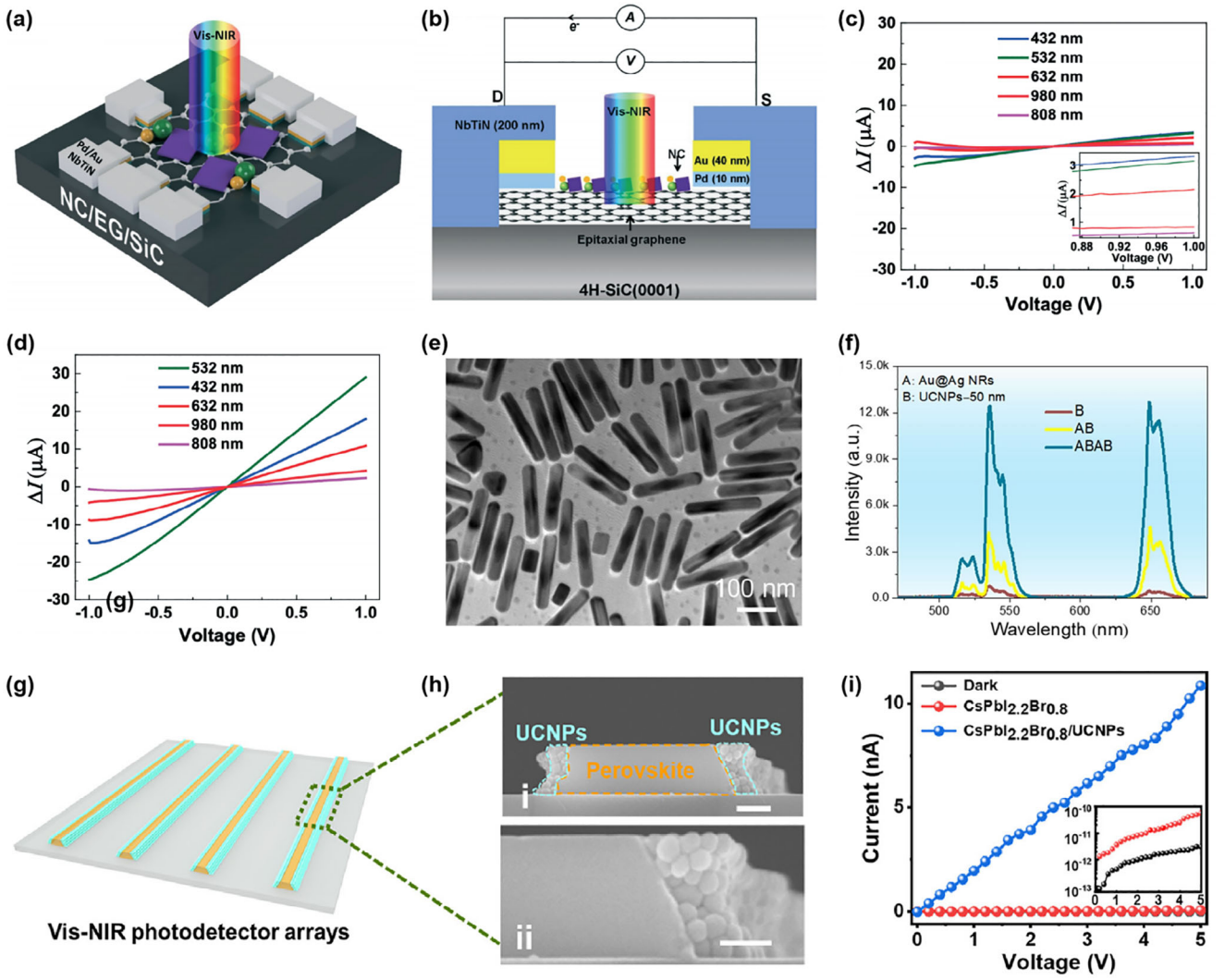

Figure 6. The UCNP-based photodetectors. a) 3D schematic of the NC/EG/SiC-based hybrid photodetector. b) Side view of the NC/EG/SiC based hybrid photodetector. c,d) Photocurrent as a function of applied V_{DS} for PB/EG/4H-SiC and NC/EG/SiC hybrid devices under broad-range wavelength illumination (432–980 nm). e) TEM image of Au@Ag nanorods. f) The typical upconversion emission of Er^{3+} under illumination at 980 nm of different structures. g) Schematic diagram of the vis–NIR $CsPbI_{2.2}Br_{0.8}$/UCNPs photodetector arrays. h) Cross-section SEM images of the 1D side-wrapped $CsPbI_{2.2}Br_{0.8}$/UCNPs structure (scale bars, i: 200 nm, ii: 100 nm). i) Dark current and photocurrent of $CsPbI_{2.2}Br_{0.8}$ photodetectors and $CsPbI_{2.2}Br_{0.8}$/UCNPs photodetectors under the illumination of a 980 nm laser. a–d) Reproduced with permission.[122] Copyright 2022, Wiley. e,f) Reproduced with permission.[124] Copyright 2022, Royal Society of Chemistry. g–i) Reproduced under the terms of the CC-BY Creative Commons Attribution 4.0 International license (https://creativecommons.org/licenses/by/4.0).[125] Copyright 2022, The Authors, published by American Chemical Society.

4.2.1. Three-Terminal Photonic Flash Memory

Three-terminal flash memory shares a similar architecture with the class field-effect transistor, with the key difference being the addition of a floating gate layer into the gate-dielectric layer. During the programming operation, charges tunnel from the channel region into the chargeable floating gate or trapping layer.[128] The stored charges are released back to the semiconductor channel by applying a reverse bias to the gate electrode, realizing the erase operation.[129] These two processes primarily rely on charge tunneling effects, such as Fowler–Nordheim tunneling or direct tunneling. This mechanism allows for optical control of data storage, enabling multilevel memory.[130] For three-terminal flash memory, the selection of materials has a crucial impact on performance, reliability, and cost. First, the proper height and width of the barrier can effectively regulate the injection and release of charges in the floating gate, ensuring reliable data storage.[108] In addition, the material should have excellent charge trapping capability to prevent the stored charges in the floating gate from escaping, thereby maintaining long-term nonvolatility. Key parameters such as memory window, data retention time, and programming/erasing speed further determine the storage capacity, stability, and operational speed of the device, making them essential considerations in material and device design.

Moreover, in three-terminal photonic flash memory, the charge state of the floating gate can be modulated not only by gate-voltage-induced charge tunneling but also by photogenerated carriers under optical signals.[131] With high speed,

broad bandwidth, and optical information storage and processing capabilities, photonic flash memory addresses limitations of traditional memory, such as speed bottlenecks, low energy efficiency, and encryption challenges.[7] These advantages position photonic flash memory as a promising technology for optical sensing, image capture, and photonic neuromorphic computing. However, most photonic flash memories currently rely on short-wavelength light excitation, highlighting the significant application potential of UCNPs capable of sensing NIR in photonic flash memory devices.[34] By combining with other materials such as P3HT, UCNPs can harness the energy generated by NIR to induce the formation of electron–hole pairs, which in turn modulate the charge state of the floating gate, enabling optical gate control.

To enable NIR-excited data writing, our group utilized $NaYF_4$/Er@$NaYF_4$ doped P3HT as the semiconductor layer of the transistors.[49] Since the absorption band of P3HT (400–700 nm) overlaps with the main emission peak of $NaYF_4$/Er@$NaYF_4$ UCNPs, upon NIR excitation, the UCNPs emit photons that are absorbed by P3HT, generating electron–hole pairs within the semiconductor. As a result, 980 nm laser-assisted programming process can expand the memory window and realize robust multilevel storage. Furthermore, to extend this NIR-modulated multilevel memory to retinomorphic devices that simultaneously perceive and encode narrow IR spectral information, our group recently further modified the device configuration and successfully simulated synaptic responses using a UCNPs@SiO_2/P3HT transistor (**Figure 7a**).[44] The spectral characterization in Figure 7b,c further validates the efficient radiative energy transfer between the UCNPs and P3HT, as previously discussed. During the programming process, a sufficiently large positive bias drives electrons from the P3HT layer to the SiO_2, where they are ultimately captured by the UCNPs. These captured electrons generate a built-in electric field that accelerates the accumulation of holes in the semiconductor layer, leading to a threshold voltage shift. According to the energy-level structure, the SiO_2 barrier at the interface blocks the trapped electrons, functioning as a potential well and ensuring long-term memory storage. By optimizing the silica shell thickness, a delicate balance is struck between enhancing programming speed and data retention. In addition, as the programming time increases, the number of generated charge carriers also increases, and the storage window expands, demonstrating the device's potential for multilevel storage (Figure 7d). Moreover, when NIR pulses are applied to the device, the generation of photo-induced charge carriers leads to typical short-term potentiation behavior. Notably, the programming process of the device can influence the response to NIR light. We explore the synergistic effect of NIR irradiation and electrical programming operations (S1–S8) on synaptic response, further confirming that the physical reservoir exhibits high-dimensional storage characteristics through electrical programming as presented in Figure 7e.

In another study, we utilized MoS_2 as the photo-sensitive material to design a NIR-responsive flash memory based on a UCNPs-MoS_2 floating-gate phototransistor (Figure 7f).[35] In this device, under NIR illumination, the upconversion process excites holes in MoS_2 are transferred to pentacene due to band bending (Figure 7g), while the remaining electrons are localized in MoS_2 by the interfacial barrier, achieving effective carrier separation. The absorption spectrum and the PL spectrum further demonstrated a good spectral match between MoS_2 and Ln^{3+} doped $NaYF_4$ UCNPs (Figure 7h), which is consistent with the analysis in the previous chapter. As shown in Figure 7i, this synaptic transistor exhibits a stable photoelectric response, enabling NIR-driven writing and electrical erasing capabilities. Besides, similar to MoS_2, the organic material pentacene also exhibits excellent performance in optoelectronic conversion and light sensing, with a broad absorption spectrum.[33] Figure 7j proves that when combined with UCNPs, pentacene also demonstrates charge carrier capture and multilevel data storage capabilities. This heterojunction design not only enhances the device's sensitivity to NIR light but also enables a persistent photocurrent effect, paving the way for multilevel storage and efficient information retention, making it an ideal choice for the fabrication of three-terminal photonic flash memory.

4.2.2. Two-Terminal Photonic Memristor

Two-terminal memristors feature a switching medium sandwiched between electrodes, enabling compact integration and efficient on-chip implementation.[5] The switching medium layer can be dynamically reconfigured in response to external stimuli, such as electric fields, magnetic fields, or light, resulting in changes of conductivity or resistance state.[132,133] In recent years, the development of memristors has made rapid progress, which exhibit a wide range of resistive switching behaviors, including abrupt (digital) or gradual (analog) processes.[134] These resistance switching behaviors make memristors ideal candidates for neuromorphic systems that mimic the way the human brain processes and stores information.[135] The resistive switching mechanism primarily relies on the formation and rupture of conductive filaments or charge trapping/detrapping at the interface, while in photonic memristors, optical excitation further modulates these processes via the photovoltaic effect, photogating effect, or photon-assisted carrier migration.[136] Key performance parameters include the ON/OFF ratio, which determines the contrast between resistive states, retention time and endurance, which indicate memory stability, and response speed, which defines the switching efficiency.

Compared to traditional electrical memristors, photonic memristors offer faster switching speeds, higher energy efficiency, and greater flexibility through light-controlled conductance, enabling multi-channel information processing.[6,137] This is particularly beneficial for optical computing and high-speed data processing, where the integration of optical and electrical signals provides higher bandwidth and lower latency, driving the advancement of optoelectronic neuromorphic computing.[138] While, a common limitation of photonic memristors is their lower NIR sensitivity compared to UV–vis sensitivity.[139] By incorporating UCNPs into the memristor field, the conductance of the memristors can be precise modulated using NIR light signals, not only broadening the memristor's photon absorption capability, but also enhancing the memristor's functionality for optoelectronic applications. For example, by using three different organic dyes (sensitizers I, II, III) to absorb light of different wavelengths and sequentially transfer energy, the energy is efficiently transferred to UCNPs, significantly expanding their light absorption ability in the vis-

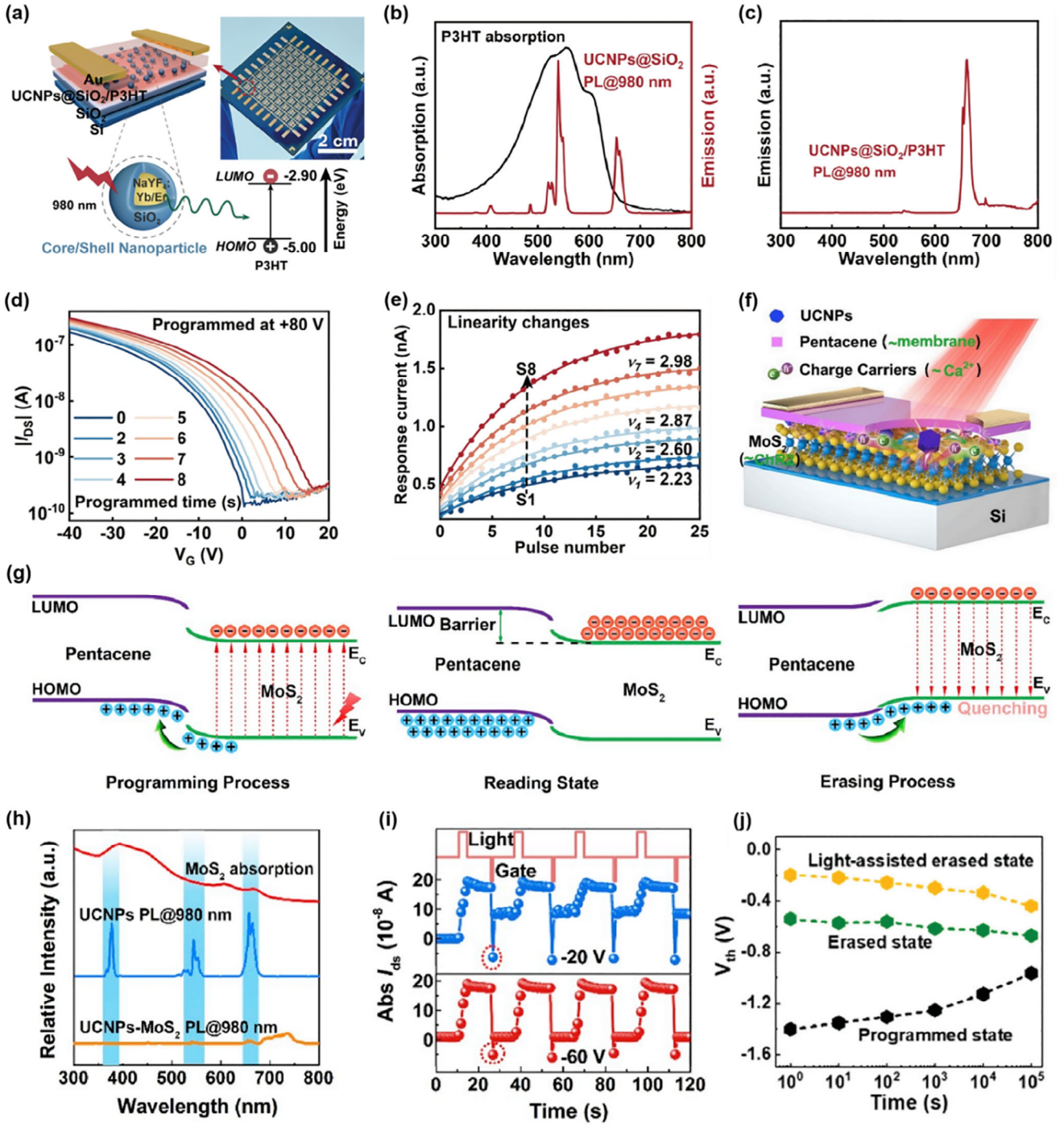

Figure 7. UCNP-based three-terminal photonic flash memory. a) Schematic diagram illustrating the device structure and radiative energy transfer process from UCNPs@SiO_2 to P3HT. b) Absorption spectrum of the P3HT film compared with the PL spectrum of UCNPs@SiO_2. The PL spectrum of UCNPs@SiO_2 embedded within the P3HT film. d) Transfer curves of the device after writing and erasing operations ($V_{DS} = -20$ V). The devices' transfer characteristic curves exhibited a positive shift with increasing programmed time due to the enhanced carrier capture state. e) Response current as a function of the number of applied light pulses under varying storage states. f) Schematic representation of a NIR artificial synaptic device utilizing a UCNPs-MoS_2 floating gate phototransistor. g) Analysis of programming process. h) UV–vis absorption spectrum of MoS_2 (red line), the PL spectrum of UCNPs (blue line), and UCNPs-sensitized MoS_2 system (purple line) under 980 nm NIR excitation. i) The source–drain current (I_{DS}) plotted as a function of time during 980 nm NIR programming process, accompanied by erasing operations at different gate pulse (20 and 60 V). j) Retention performance of a multilevel NIR photonic memory device. a–e) Reproduced under the terms of the CC-BY Creative Commons Attribution 4.0 International license (https://creativecommons.org/licenses/by/4.0).[44] Copyright 2024, The Authors, published by Wiley-VCH. f–i) Reproduced with permission.[35] Copyright 2019, Elsevier. j) Reproduced with permission.[33] Copyright 2021, Royal Society of Chemistry.

ible to NIR range.[85] These sensitized UCNPs combined with UV-responsive photoacid generators (PAG) form a memristor that acts as a light-triggered chemical destruction layer. Upon exposure to UV, vis, or NIR, the PAG is activated to release acid, rapidly corroding the storage device and ensuring the data becomes irrecoverable (**Figure** 8a–c).

Furthermore, our research group reported a NIR-responsive photonic memristor based on MoS_2-$NaYF_4$:Yb/Er UCNPs as the memristive layer, and the top and bottom electrodes are Al and ITO, respectively (Figure 8d).[36] According to the energy band alignment as shown in Figure 8g, the hole injection barrier is much lower than the electron injection barrier. At low applied voltage, only a small number of free charge carriers can cross the barrier and are trapped in the MoS_2-UCNPs. However, under the combined action of NIR light and large voltage, the photogenerated excitons are separated in the MoS_2-UCNPs interface. A large number of additional holes quickly fill the trapping sites and allow carriers to move freely, thereby switching the device from high-resistance state (HRS) to low-resistance state (LRS). Notably, as the NIR intensity increases, more photogenerated carriers are generated, resulting in higher conductivity and a lower set voltage (Figure 8e). Therefore, by integrating UCNPs into memristive devices, the device's resistance states are modulated using NIR light, enabling multilevel storage and ensuring stable memory performance (Figure 8f). In summary, distinguished from traditional neuromorphic devices, the integration of UCNPs enables NIR-modulated neuromorphic devices. By combining UCNPs with other materials, these novel neuromorphic devices can perform complex computation and storage operations under diverse external stimuli, including NIR light and electricity. Most importantly, the use of noninvasive NIR provides a foundation for implantable synaptic devices and biological neuromorphic computing in the future.

5. NIR Modulated Neuromorphic Computing

Inspired by the architecture and functionality of biological neural networks, neuromorphic computing offers a revolutionary approach to processing information. It challenges the traditional von Neumann architecture by integrating perception, memory, and computation into a single system, minimizing the need for complex signal exchange and enabling energy-efficient, parallel data processing.[140,141] Neuromorphic computing has advanced rapidly in recent years, driven by the combination of emerging hardware technologies, such as memristors, and the development of innovative artificial neural network architectures.[142,143] As a result, neuromorphic computing is progressively expanded to diversified application fields, such as real-time pattern recognition, autonomous robotics, and edge artificial intelligence.[144] Compared to traditional electrical methods, optical modulation in neuromorphic computing utilizes the low energy consumption and multimodal characteristics of light to achieve high-speed signal transmission, enhanced bandwidth, and reduced crosstalk.[145] It meets the demand for computing power in the fields of artificial intelligence and deep learning in a more efficient and flexible way.[146] The hardware-implemented NIR neuromorphic computing typically relies on advanced optoelectronic devices, such as three terminal photonic synaptic transistors and photonic memristors.

Three terminal photonic synaptic transistors regulate the conductivity of channels through optical signals, enabling dynamic adjustment of synaptic weights.[147] These devices integrate sensing, storage, and computing functions, simulating the behavior of biological synapses.[109] In addition, photonic memristors can store multilevel weight information by modulating the resistance states with optical signals, further enhancing the capability of neuromorphic systems to process and store information efficiently.[148] NIR machine vision is essential for a range of advanced applications, such as night vision systems for military operations, in vitro intraoperative diagnostics, and enhancing human visual perception beyond the visible spectrum to detect nighttime hazards. However, common crystalline materials like silicon and compound semiconductors are unable to detect infrared signals without filters due to their large bandgap. The absence of intelligent devices capable of simultaneously perceiving, filtering, storing, and processing NIR signals has hindered the advancement of NIR-excited neural networks. The UCNP-based optoelectronic memory devices overcome the large bandgap limitation of traditional materials, enabling direct detection of infrared signals without filters. This breakthrough positions it as an ideal candidate for addressing above challenges effectively. By modifying the composite material and structure, these devices can be tailored to exhibit different properties, making it suitable for different artificial neural networks (ANNs).[149]

This section explores the role of brain-inspired ANNs in neuromorphic computing, with a focus on three types of neural networks such as CNNs[150] and RC.[151] We explore how the performance (such as response speed, nonlinear behavior, and memory retention) of UCNP-based devices are optimized to better meet the requirements of these neural networks, thereby enhancing computational efficiency, expanding functionality, and improving the capability to mimic biological functions. Our research group have developed UCNP-based synaptic transistors with optoelectronic and memory functions, which demonstrated unique advantages in CNNs and recurrent neural networks (RNNs),[152] respectively.

5.1. Convolutional Neural Networks

CNNs are a deep learning model mainly used for image and video analysis, which has the characteristics of local connections and weight sharing.[153] Generally, CNNs consist of convolutional layers, pooling layers, and fully connected layers, which simulate the functions of the human visual system through convolution operations and feature extraction mechanisms (**Figure** 9a).[154] CNNs relying on long-term potentiation (LTP) and long-term depression (LTD) for efficient learning and memory retention.[155] LTP strengthens neural connections, while LTD weakens them, simulating the biological processes of learning and forgetting. Synaptic devices function as weight storage and computation units in CNNs, primarily utilized in convolutional and fully connected layers, effectively replacing traditional numerical storage and matrix multiplication operations.[156] In the optoelectronic synaptic devices based CNNs, the intensity, wavelength, or frequency of optical signals can be adjusted to modulate the conductivity state of the synaptic devices, thereby enabling effective weight updates.[157] Meanwhile, kernel cells utilize the architecture of

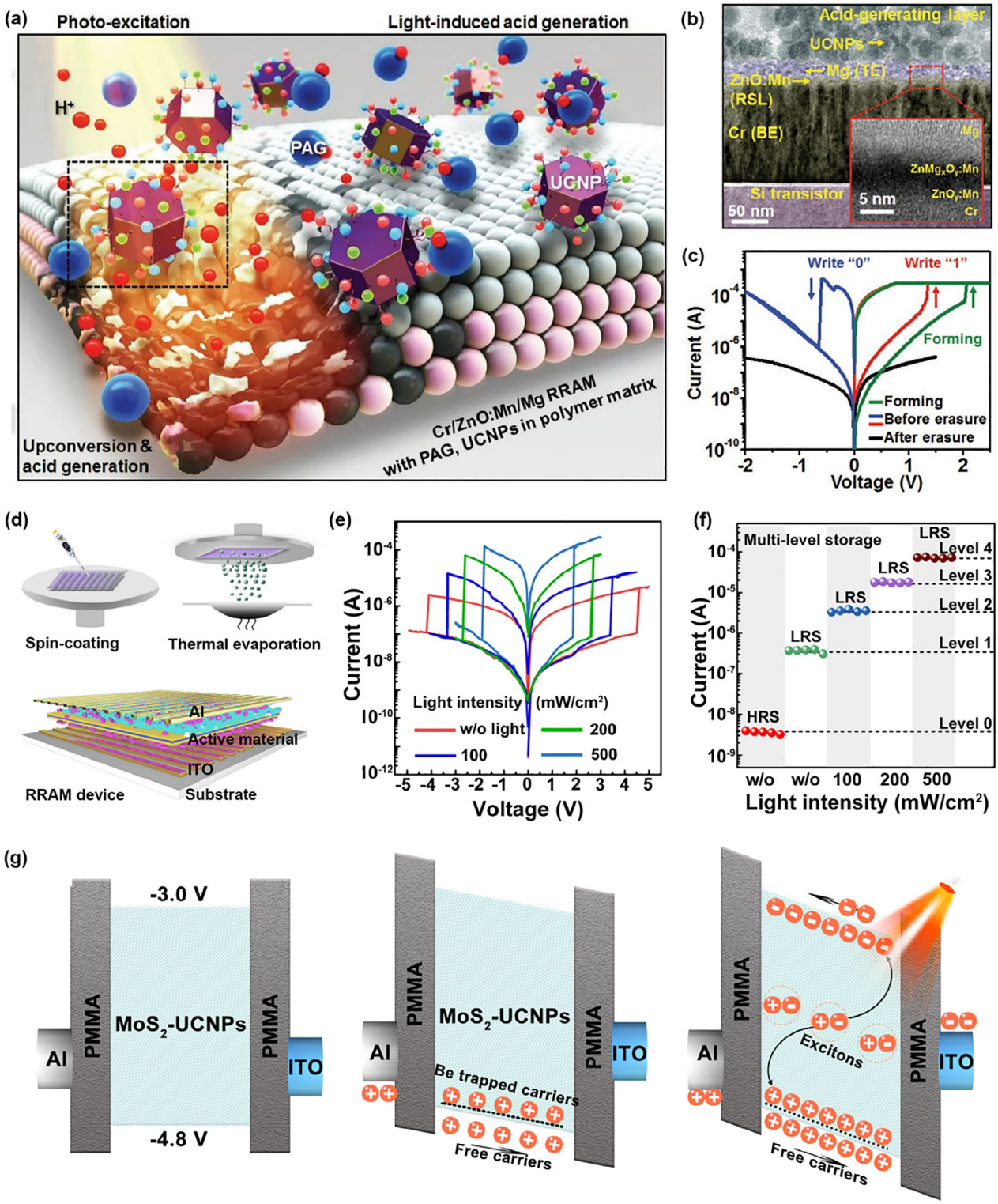

Figure 8. The UCNP-based two-terminal photonic memristors. a) Schematic illustration of the photo-induced irreversible data erasure in ultrathin nonvolatile memory device based on UCNPs. b) Cross-sectional TEM image of the integrated system, showing the RRAM on the Si transistor coated with UCNPs/PAG/PEO layer. c) *I–V* characteristic curves of the Cr/ZnO:Mn/Mg RRAM device before and after photo-induced chemical destruction. d) Schematic illustration of the MoS_2-UCNP-based RRAM device and its main fabrication process. e) Typical *I–V* curves of the RRAM device measured under different NIR light intensity. f) Multilevel storage states of the RRAM device obtained through different light illuminations. g) Energy band diagram of device at initial state, during LRS process under dark condition, and the LRS process under 980 nm NIR illumination. a–c) Reproduced with permission.[85] Copyright 2016, Wiley. d–g) Reproduced with permission.[36] Copyright 2018, Wiley.

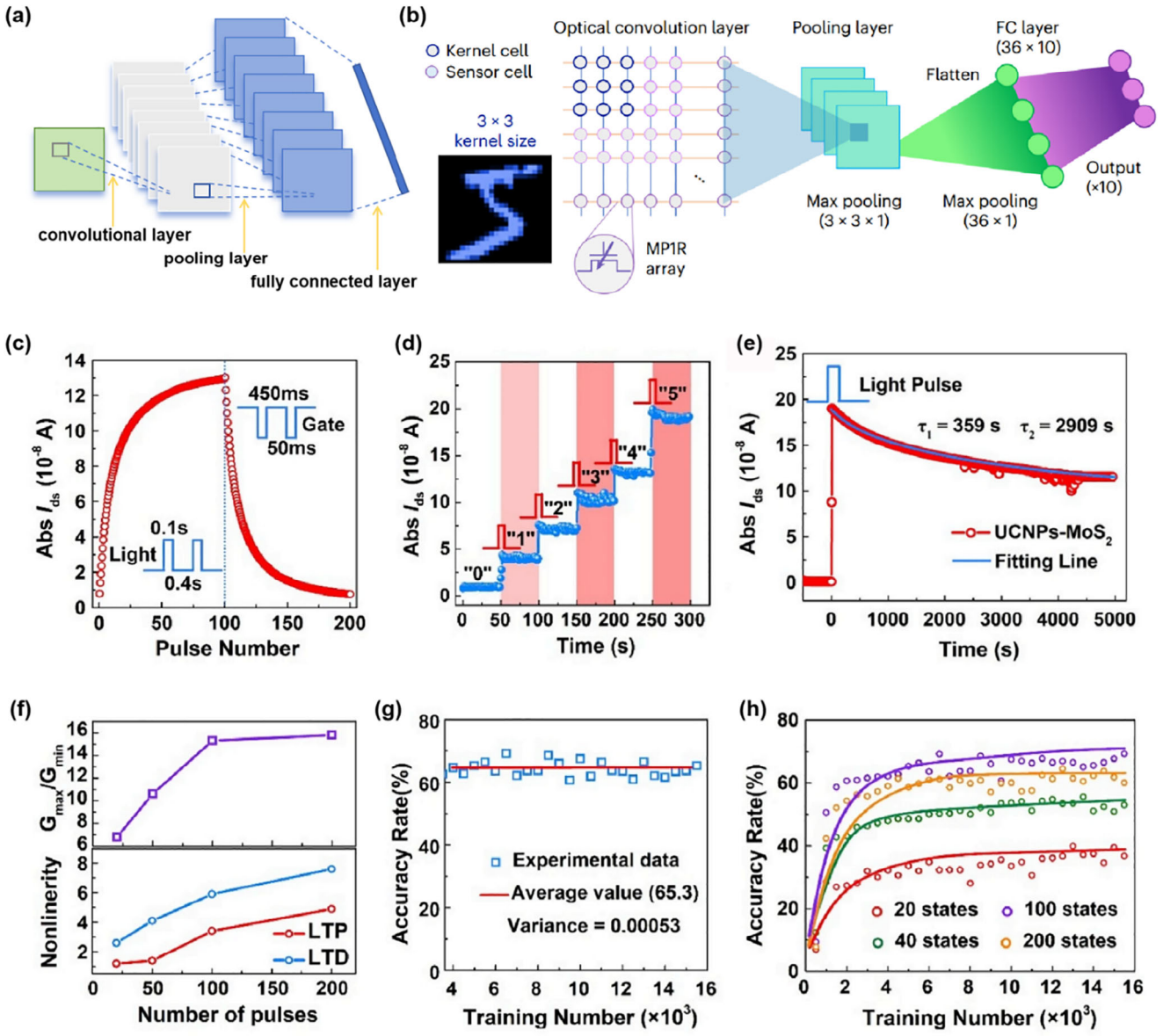

Figure 9. a) Simplified schematic of CNNs. b) Schematic diagram of handwritten digit recognition by MP1R array based optical CNNs. c) Single LTP/LTD triggered by 100 continuous light pulses (potentiation) and voltage pulses (depression).Temporal I_{DS} curves in UCNPs-sensitized MoS_2 with NIR light programming. d) Multilevel storage is achieved through different light intensity programming processes. e) Temporal I_{DS} curves in UCNPs-sensitized MoS_2 with NIR light programming. f) Calculated G_{max}/G_{min} value as a function of pulse number (top), and the nonlinearity degree of LTP and LTD as a function of pulse number (bottom). g) The recognition accuracy rate of our artificial neuromorphic network. h) The accuracy rates for the case of different weight states. b) Reproduced with permission.[160] Copyright 2024, Springer Nature. c–h) Reproduced with permission.[35] Copyright 2019, Elsevier.

synaptic arrays to perform feature extraction operations, accelerating data processing through convolution with weight matrices. Architectures based on synaptic arrays facilitate large-scale parallel operations, thereby efficiently implementing convolutional and fully connected computations in CNNs.[158] Therefore, to implement CNNs efficiently using neuromorphic devices, particularly optoelectronic devices, the following features are essential: (i) Long-term retention characteristics: Devices should demonstrate long-term retention of weight changes to maintain the integrity of stored information and minimize reprogramming frequency. (ii) High dynamic range: Neuromorphic devices should allow for dynamic weight updates with simple control mechanisms, reducing energy consumption and enhancing efficiency in tasks such as convolution and weighted summation. (iii) High linearity and symmetry: Conductivity modulation must have high linearity and symmetry to support accurate weight updates, ensuring computational precision. Therefore, only nonvolatile synaptic devices with long-term memory capabilities, high linearity and symmetry of LTP/LTD, and high computational efficiency are suitable for CNNs. They can dynamically update weights through simple control mechanisms and can be effectively applied in the training process of CNNs.[159]

The CNNs based on a multi-phototransistor and one-memristor (MP1R) array constructed by Yang et al. successfully achieved recognition of handwritten digits, but it is still limited to Vis light excitation (Figure 9b).[160] To broaden the excitation band of phototransistors to the NIR spectrum, we designed a NIR-responsive synaptic device based on the upconversion effect in 2020. Since UCNPs materials lack a persistent photocurrent effect, it is crucial to carefully select materials that pair with UCNPs. These materials should possess not only strong optoelectronic conversion capabilities but also the ability to capture charges for nonvolatile storage, enabling the device to demonstrate LTP characteristics. In the previous sections, we have discussed the MoS_2 material, which can facilitate efficient charge transport within the material and minimize recombination losses.[35] Therefore, using UCNPs-MoS_2 as the floating-gate layer in photonic flash memory allows NIR to modulate the Vis light emitted by UCNPs, further controlling the light absorption behavior of the MoS_2. When continuous NIR light pulses are applied, photogenerated electrons accumulate in the MoS_2 layer, while the photogenerated holes are transferred to channel, resulting in a continuous increase in the device's conductivity. Conversely, when continuous negative voltage pulses are applied, the electrons accumulated in the MoS_2 layer due to the optical grating can be erased, leading to a continuous decrease in conductivity. These two processes correspond to LTP/LTD behavior as shown in Figure 9c.[35] Furthermore, photogenerated electrons can be located in MoS_2 even after switching off the light due to the energy barrier, which ensures a long charge storage capacity, resulting a persistent photocurrent effect (Figure 9d,e). Based on the LTP/LTD characteristics of this optoelectronic device, a supervised learning model using a single-layer perceptron CNNs is simulated. The network's output value is obtained by performing a multiplication of the input vector and the synaptic weight matrix, followed by transformation through a sigmoid activation function. By controlling the number of LTP/LTD pulses, both the linearity and the change rate of the conductance states can be balanced (Figure 9f), thereby enhancing the precision of weight updates in the network. These characteristics enable our synaptic devices to exhibit high recognition accuracy in light controlled neural network. This work offers new perspectives on the application of novel NIR-responsive synaptic devices in neuromorphic computing (Figure 9g,h).

5.2. Reservoir Computing

As a derivative of the RNNs model, RC has a simpler training process, lower power consumption, and faster computation.[161] Mainly because it utilizes the nonlinear dynamics of the reservoir to convert the input signal into high-dimensional space, effectively capturing temporal features without iterative weight updates within the reservoir itself.[162,163] The simplicity of this training not only improves the computing efficiency, but also makes RC very suitable for resource limited edge computing, internet of things, bionic visual simulation and other fields.[164,165] RC networks typically consist of three layers: an input layer, a reservoir layer, and an output layer (**Figure 10a**).[166] Synaptic devices provide nonlinear response and state preservation, and are the core components in the reservoir layer that serve as dynamic processing and weight storage.[167] However, physical RC systems for intelligent NIR sensing are still insufficient due to their limited expressive power and inability to directly detect NIR signals without filters.[168] Therefore, to explore a filter free NIR device with high expressive power, nonlinear response, short-term memory (STM), multiple states, and large dynamic range as a dynamic reservoir with infrared control, it is essential to exhibit the following three features:

1) Relaxation tunability: Relaxation tunability refers to the ability of a device to adjust the time scale over which its response signal returns to the initial state after stimulation.[169] This property directly influences the dynamic behavior of the reservoir layer and is crucial for effectively processing time-series inputs.
2) Fading memory: Fading memory, essential in RC, allows a device to temporarily retain input features that gradually decay. Driven by input pulse frequency or intensity, this nonlinearity enables time-dependent signal encoding, linking the output state to the temporal distribution of the input.

In NIR-light-activated synaptic devices, relaxation tunability can be achieved through (i) photogenerated charge capture and release, (ii) an interface heterojunction, and (iii) generation of metastable excitons by NIR light excitation in specific materials. UCNPs can generate metastable excitons under NIR light excitation. Optimized UCNP-based devices maintain the desirable properties of traditional UCNPs while also offering enhanced functionalities. These devices are poised to enable low-cost, RC-based edge learning and unlock the potential for artificial infrared perception.

To bridge the gap in NIR-modulated optoelectronic devices for RC applications, our team recently developed a retinal morphology device modulated by NIR light, which can simultaneously perceive and encode narrow NIR wavelength data.[44] This device is based on a core–shell structured UCNPs@SiO_2 and P3HT nanocomposite materials, which serve as the channel in phototransistors (Figure 10b). This three-terminal photonic transistor comprises a semiconductor channel, a photosensitive layer, a charge trapping layer, and a tunnel dielectric layer. First, UCNPs are blended with P3HT, as illustrated in Figure 7a,b. The strong absorption band of p-type P3HT overlaps with the emission peaks of UCNPs@SiO_2, enabling high-energy photons upconverted by UCNPs to be absorbed by P3HT, thereby generating photoinduced electron–hole pairs. In addition, the silica shell not only suppresses nonradiative energy loss and enhances NIR light responsiveness but also acts as a tunnel dielectric layer, capturing electrons to extend the storage time of photogenerated charges. This provides temporal correlation essential for the reservoir layer. Furthermore, the composite structure forms a heterojunction, where the energy band barrier at the interface prevents rapid recombination of charge carriers. This prolongs the charge recombination time, enabling dynamic adjustment of the relaxation time. Devices with different electrical properties exhibit programmed state changes in synaptic responses under NIR radiation, a characteristic ideal for achieving

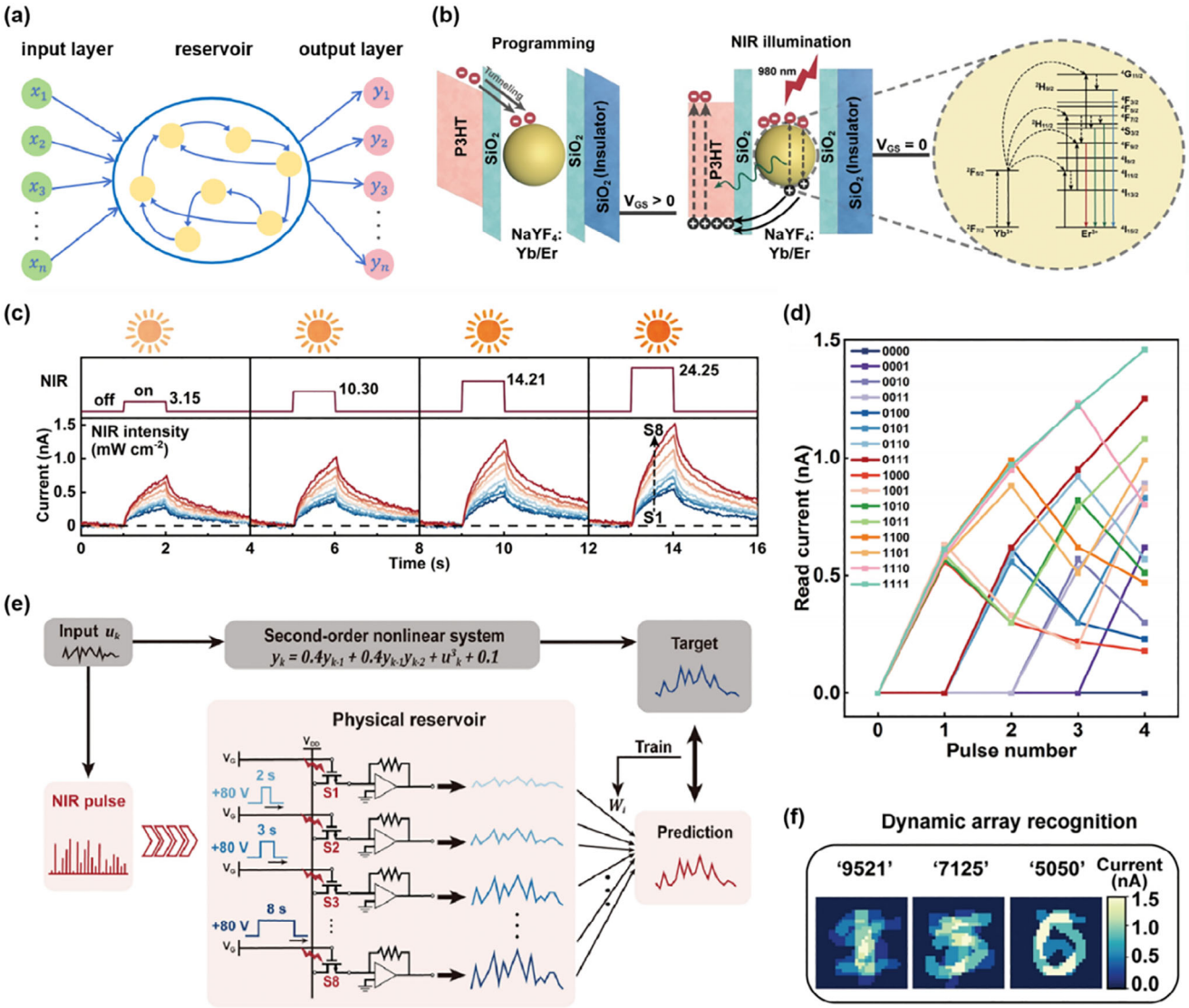

Figure 10. a) Simplified schematic of RC. b) The energy scheme of the device during an electrical programming behavior and NIR illumination operation. The yellow area demonstrates the energy level of UCNPs and the corresponding working mechanism under NIR illumination. c) The current response after applying NIR pulses of varying intensities under different device storage states. d) Current responses from the reservoir drained into 16 pulse streams. e) The schematic of the task calculated using the UCNPs@SiO_2-based reservoir. f) Three examples of reservoir states in the dynamic handwritten array, illustrating differences in reservoir state. b–f) Reproduced under the terms of the CC-BY Creative Commons Attribution 4.0 International license (https://creativecommons.org/licenses/by/4.0).[44] Copyright 2024, The Authors, published by Wiley-VCH.

high-dimensional RC (Figure 10c). In summary, this study leverages the synergistic effects of photovoltaic and photochemical mechanisms to achieve photon–electron coupling dynamics. This results in high-dimensional, nonlinear data processing, ensuring high accuracy in subsequent RC calculations (Figure 10d). To evaluate the computational capability of our prepared hardware implemented RC system, we used a second-order nonlinear dynamic equation task (Figure 10e). As a result, the recognition accuracies for the static and dynamic handwritten digit NIR images reach 91.13% and 90.07%, respectively (Figure 10f). These results underscore the potential of NIR based in-sensor RC systems as powerful tools for future computation and prediction in sequential tasks.

6. Conclusions and Perspective

In summary, this review highlights the latest advancements in UCNP-based optoelectronic devices, emphasizing strategies for designing UCNP-based composites to enhance the performance of various optoelectronic applications, including NIR-responsive photodetectors, three-terminal photonic flash memory, and two-terminal photonic memristors. In view of the great potential of NIR-modulated neuromorphic devices in the integration of sensing, storage and computing, we examine the relationship between key device characteristics (e.g., response speed, nonlinear behavior, memory retention, etc.) and various neural networks (including CNNs and RC). The ultimate goal

is to facilitate the on-demand design of NIR-controlled optoelectronic devices tailored to meet specific application requirements.

While significant progress has been made, several critical challenges remain in fully harnessing the potential of UCNPs. One of the primary obstacles is achieving higher quantum yields at low-power excitation,[170] which is a crucial factor for improving efficiency and enabling practical applications. Overcoming this challenge requires the development of novel materials and innovative doping strategies that enhance the absorption and emission properties of UCNPs. Another significant hurdle is enhancing the stability of UCNPs, particularly under prolonged exposure to environmental conditions such as temperature fluctuations, moisture, and radiation.[171] Strategies to increase the chemical and photostability of UCNPs, such as advanced core–shell engineering and the use of protective coatings, must be explored.[74] Furthermore, minimizing nonradiative losses through optimized material design will be essential in maintaining efficient upconversion under real-world operating conditions. Further research should also prioritize refining doping techniques and developing novel core–shell architectures, as well as exploring the precise spatial control of dopant ions.[172] Advanced ion-implantation methods and atomic-scale control over doping could also pave the way for designing highly tunable materials with enhanced upconversion performance. These advancements could unlock new possibilities for maximizing upconversion efficiency and expanding the range of UCNP-based applications.

In parallel, the practical deployment of UCNPs in fields such as implantable neuromorphic systems and optical communication modules requires overcoming significant challenges in material biocompatibility.[173] Developing UCNPs that are biocompatible, nontoxic, and able to function effectively in living systems will be crucial for medical and health-related applications. Moreover, the miniaturization of UCNP-based devices, while maintaining their performance, is necessary for integration into compact, lightweight systems. Achieving robust integration with other functional materials will also be essential, as many real-world applications will require UCNPs to work seamlessly in multi-material systems, such as hybrid photonic circuits or bio-integrated devices. Tackling these challenges will require interdisciplinary efforts, combining advancements in material science, nanotechnology, and device engineering.[174] As we look toward the future, UCNPs are poised to play a transformative role in several frontier fields, including electronic eyes, implantable devices, optical memory, and neurocomputing, leveraging their unique properties such as NIR sensing and tunable excitation wavelengths (**Figure 11**).

i. In the domain of electronic eye technologies, UCNPs hold transformative potential for advancing vision systems, particularly in optimizing light-to-electrical signal conversion under low-light conditions. By leveraging UCNPs' NIR-responsive properties, these systems could bypass direct photoreceptor stimulation, enhance ambient light utilization efficiency. Unlike infrared imaging, which relies on passive thermal radiation detection, UCNPs-enhanced electronic eyes actively convert NIR into visible light, enabling adaptive spectral tuning and localized energy transfer for improved visual signal processing and potential high-resolution optical perception.

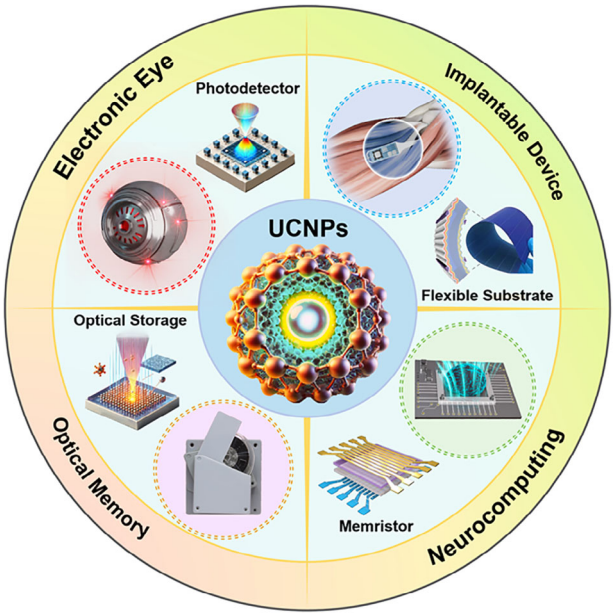

Figure 11. Schematic illustration of the potential applications of UCNPs in future technologies. Image for "Flexible Substrate": Adapted with permission.[180] Copyright 2024, Springer Nature.

ii. In the domain of implantable photoelectric medical devices: UCNPs demonstrate immense potential through their integration into flexible, microscale systems. Their biocompatibility, combined with the ability to operate under NIR excitation, makes UCNPs ideal for developing minimally invasive implantable devices. These devices could facilitate continuous, noninvasive monitoring of critical health parameters or even enable on-demand therapeutic interventions, offering a new level of personalization in healthcare. Flexible UCNP-based sensors could be used for a variety of applications, from monitoring glucose levels to providing real-time feedback in neural stimulation therapies, marking a significant step forward in medical device innovation.

iii. In the field of optical memory: UCNPs present a promising foundation for developing high-capacity, secure data storage systems. Their ability to store and retrieve optical information in a nonvolatile manner opens up new avenues for advancements in optical memory and secure data storage technologies. UCNP-based optical storage could offer superior storage density, data security, and faster read–write speeds compared to current technologies, positioning UCNPs as a key material for next-generation storage solutions.

iv. In the realm of neuromorphic computing: UCNPs could play a pivotal role in developing energy-efficient, light-controlled neural network systems such as spiking neural networks (SNNs).[175,176] SNNs process information through discrete spike-based communication, closely mimicking biological neural behavior.[177] A key challenge in hardware implementation is designing optoelectronic devices that can efficiently couple optical signals with neuronal spiking dynamics.[178] While UCNP-based devices hold great potential for

coupling optical signals with these dynamics through their NIR-excited response, achieving precise control over light pulse timing and intensity remains a significant hurdle. Future advancements in integrating UCNPs with threshold-switching memristors and phototransistors could enable efficient spike encoding and adaptive learning in optoelectronic neuromorphic systems. This breakthrough has the potential to enhance artificial intelligence and machine learning systems, driving innovations in brain-like computing and revolutionizing fields such as robotics, cognitive computing, and autonomous systems.[179]

Overall, UCNP-based optoelectronic devices have immense potential to drive innovation across various technological frontiers. With continued advancements in material design, doping strategies, and device integration, UCNPs are positioned to play a pivotal role in the development of prosthetic technologies, implantable medical devices, optical memory, and neuromorphic computing. Addressing challenges related to stability, biocompatibility, and efficiency will be key to unlocking their full potential and broadening their applications in next-generation technologies.

Acknowledgements

S.-T.Han acknowledges the financial support from the Hong Kong Research Grants Council, Young Collaborative Research Grant (C5001-24), Research Institute for Smart Energy and Guangdong Provincial Department of Science and Technology (2024B1515040002). Y. Zhou acknowledges grants from RSC Sustainable Laboratories Grant (L24-8215098370), the Science and Technology Innovation Commission of Shenzhen (JCYJ20220818100206013), RSC Researcher Collaborations Grant(C23-2422436283), State Key Laboratory of Radio Frequency Heterogeneous Integration (Independent Scientific Research Program No. 2024010), and NTUT-SZU Joint Research Program. This work was also supported by the National Natural Science Foundation of China (52373248), Guangdong Provincial Department of Science and Technology (2024A1515010006, and 2024A1515011718), Guangdong Basic and Applied Basic Research Foundation (2023A1515012479 and 2025A1515011274), and the Science and Technology Innovation Commission of Shenzhen (JCYJ20230808105900001, JCYJ20220531102214032, 20231123155543001, and JCYJ20240813141813018).

Conflict of Interest

The authors declare no conflict of interest.

Keywords

neuromorphic computing, NIR-optoelectronic devices, photodetectors, photonic memristors, upconversion nanoparticles

Received: December 15, 2024
Revised: February 21, 2025
Published online:

[1] Q. Q. Ren, C. Y. Zhu, S. J. Ma, Z. Q. Wang, J. M. Yan, T. Q. Wan, W. C. Yan, Y. Chai, *Adv. Mater.* **2024**, *36*, 2407476.
[2] J. J. Zha, S. H. Shi, A. Chaturvedi, H. X. Huang, P. Yang, Y. Yao, S. Y. Li, Y. P. Xia, Z. M. Zhang, W. Wang, H. D. Wang, S. C. Wang, Z. Yuan, Z. B. Yang, Q. Y. He, H. L. Tai, E. H. T. Teo, H. Y. Yu, J. C. Ho, Z. R. Wang, H. Zhang, C. L. Tan, *Adv. Mater.* **2023**, *35*, 2211598.
[3] H. Ding, G. Q. Lv, X. Cai, J. Y. Chen, Z. Y. Cheng, Y. X. Peng, G. Tang, Z. Shi, Y. Xie, X. Fu, L. Yin, J. Yang, Y. T. Wang, X. Sheng, *Light: Sci. Appl.* **2022**, *11*, 130.
[4] Z. C. Li, B. L. Zhang, Z. H. Zhang, J. C. Bünzli, A. B. Yusoff, Y. Y. Noh, P. Gao, *Mater. Sci. Eng., R* **2023**, *152*, 100710.
[5] X. Z. Chen, Y. Xue, Y. B. Sun, J. B. Shen, S. N. A. Song, M. Zhu, Z. T. Song, Z. G. Cheng, P. Zhou, *Adv. Mater.* **2023**, *35*, 2203909.
[6] J. Zhou, W. Li, Y. Chen, Y. H. Lin, M. D. Yi, J. Y. Li, Y. Z. Qian, Y. Guo, K. Y. Cao, L. H. Xie, H. F. Ling, Z. J. Ren, J. P. Xu, J. T. Zhu, S. K. Yan, W. Huang, *Adv. Mater.* **2021**, *33*, 2006201.
[7] Y. Park, M. K. Kim, J. S. Lee, *Carbon* **2020**, *165*, 455.
[8] K. H. Li, X. K. Yang, Y. Lu, J. Y. Xue, S. C. Lu, J. J. Zheng, C. Chen, J. Tang, *Adv. Energy Mater.* **2022**, *12*, 2200725.
[9] Z. X. Wang, Z. Wang, D. Li, C. L. Yang, Q. C. Zhang, M. Chen, H. J. Gao, L. Wei, *Nature* **2024**, *626*, 72.
[10] J. Y. Zhu, Y. X. Li, X. Y. Lin, Y. Y. Han, K. F. Wu, *Nat. Mater.* **2024**, *23*, 1027.
[11] Q. Y. Guo, D. Z. Ji, Q. K. Wang, L. Peng, C. Zhang, Y. E. Wu, D. R. Kong, S. Luo, W. T. Liu, G. Chen, D. P. Wei, Y. Q. Liu, D. C. Wei, *Adv. Mater.* **2024**, *36*, 2406345.
[12] J. J. Wei, G. Z. Liu, H. R. Fu, W. Zheng, L. F. Ma, X. Y. Chen, *Coord. Chem. Rev.* **2024**, *519*, 216119.
[13] H. Li, Y. Kim, H. Jung, J. Y. Hyun, I. Shin, *Chem. Soc. Rev.* **2022**, *51*, 8957.
[14] M. Manley, *Chem. Soc. Rev.* **2014**, *43*, 8200.
[15] S. Norouzi, M. Sadeghi, A. Liaghat, M. Tuller, S. B. Jones, H. Ebrahimian, *Remote Sens. Environ.* **2021**, *256*, 112315.
[16] J. Tian, Z. C. Zhang, W. D. Philpot, Q. J. Tian, W. F. Zhan, Y. B. Xi, X. Q. Wang, C. C. Zhu, *Remote Sens. Environ.* **2023**, *290*, 113549.
[17] M. Kataria, K. Yadav, S. Y. Cai, Y. M. Liao, H. I. Lin, T. L. Shen, Y. H. Chen, Y. T. Chen, W. H. Wang, Y. F. Chen, *ACS Nano* **2018**, *12*, 9596.
[18] N. Liang, C. Cao, Z. L. Xie, J. X. Liu, Y. S. Feng, C. J. Yao, *Mater. Today* **2024**, *75*, 309.
[19] Y. L. Chang, H. R. Chen, X. Y. Xie, Y. Wan, Q. Q. Li, F. X. Wu, R. Yang, W. Wang, X. G. Kong, *Nat. Commun.* **2023**, *14*, 1079.
[20] Q. Q. Li, Y. P. Huang, H. Y. Zhu, Y. Q. Zhu, Y. X. Yi, X. D. Li, H. R. Chen, B. Li, D. B. Li, Y. L. Chang, *Adv. Sci.* **2024**, *11*, 2408097.
[21] R. T. Parayil, S. K. Gupta, M. Mohapatra, *Coord. Chem. Rev.* **2024**, *522*, 216200.
[22] W. H. Gao, C. Chen, *Nano Energy* **2024**, *128*, 109904.
[23] C. H. Xu, S. H. Luo, Y. Wang, X. F. Shi, C. Fu, J. Wang, C. Y. Wu, L. B. Luo, *Adv. Funct. Mater.* **2023**, *33*, 2214996.
[24] J. D. Shao, C. S. Ruan, H. H. Xie, P. K. Chu, X. F. Yu, *Adv. Sci.* **2020**, *7*, 2000439.
[25] H. U. Kim, T. Kim, C. Kim, M. Kim, T. Park, *Adv. Funct. Mater.* **2023**, *33*, 2208082.
[26] X. Zheng, R. K. Kankala, C. G. Liu, S. B. Wang, A. Z. Chen, Y. Zhang, *Coord. Chem. Rev.* **2021**, *438*, 213870.
[27] B. Chen, F. Wang, *Trends Chem.* **2020**, *2*, 427.
[28] J. Zeng, Y. F. Shang, S. W. Hao, T. Chen, Z. J. Sun, H. L. Liu, C. H. Yang, *Mater. Today Phys.* **2024**, *46*, 101520.
[29] K. Malhotra, D. Hrovat, B. Kumar, G. C. Qu, J. Van Houten, R. Ahmed, P. A. E. Piunno, P. T. Gunning, U. J. Krull, *ACS Appl. Mater. Interfaces* **2023**, *15*, 2499.
[30] H. Chen, B. B. Ding, P. A. Ma, J. Lin, *Adv. Drug Delivery Rev.* **2022**, *188*, 114414.
[31] X. Y. Ou, X. Qin, B. L. Huang, J. Zan, Q. X. Wu, Z. Z. Hong, L. L. Xie, H. Y. Bian, Z. G. Yi, X. F. Chen, Y. M. Wu, X. R. Song, J. Li, Q. S. Chen, H. H. Yang, X. G. Liu, *Nature* **2021**, *590*, 410.

[32] L. L. Xie, Z. Z. Hong, J. Zan, Q. X. Wu, Z. J. Yang, X. F. Chen, X. Y. Ou, X. R. Song, Y. He, J. Li, Q. S. Chen, H. H. Yang, *Adv. Mater.* **2021**, *33*, 2101852.
[33] H. X. Lian, Q. F. Liao, B. D. Yang, Y. B. Zhai, S.-T. Han, Y. Zhou, *J. Mater. Chem. C* **2021**, *9*, 640.
[34] W. H. Luan, Z. R. Zhao, H. Li, Y. B. Zhai, Z. Y. Lv, K. Zhou, S. M. Xue, M. Zhang, Y. Yan, Y. Cao, G. L. Ding, S.-T. Han, C. C. Kuo, Y. Zhou, *J. Phys. Chem. Lett.* **2024**, *15*, 8845.
[35] Y. B. Zhai, Y. Zhou, X. Q. Yang, F. Wang, W. B. Ye, X. J. Zhu, D. H. She, W. D. Lu, S.-T. Han, *Nano Energy* **2020**, *67*, 104262.
[36] Y. B. Zhai, X. Q. Yang, F. Wang, Z. X. Li, G. L. Ding, Z. F. Qiu, Y. Wang, Y. Zhou, S.-T. Han, *Adv. Mater.* **2018**, *30*, 1803563.
[37] S. B. Liu, Z. C. An, B. Zhou, *Chem. Eng. J.* **2023**, *452*, 139649.
[38] N. Estebanez, A. Cortés-Villena, J. Ferrera-González, M. González-Béjar, R. E. Galian, S. González-Carrero, J. Pérez-Prieto, *Adv. Funct. Mater.* **2020**, *30*, 2003766.
[39] F. Li, L. P. Tu, Y. Q. Zhang, D. X. Huang, X. X. Liu, X. R. Zhang, J. R. Du, R. W. Fan, C. H. Yang, K. W. Kraemer, J. Marques-Hueso, G. Y. Chen, *Nat. Photonics* **2024**, *18*, 440.
[40] H. B. Xia, D. Li, J. Y. Shang, Y. A. Ji, X. M. Yin, G. Q. Fang, W. Xu, B. Dong, *Adv. Funct. Mater.* **2023**, *33*, 2304045.
[41] S. B. Liu, L. Yan, J. S. Huang, Q. Y. Zhang, B. Zhou, *Chem. Soc. Rev.* **2022**, *51*, 1729.
[42] B. Amouroux, A. Eftekhari, C. Roux, J. C. Micheau, P. Roblin, M. Pasturel, F. Gauffre, C. Wuerth, U. Resch-Genger, M. Sliwa, A. Bouchet, C. Coudret, *Adv. Opt. Mater.* **2024**, *12*, 2303283.
[43] G. F. Wang, L. Li, H. D. Zheng, Q. Y. Li, J. L. Huang, L. A. Zhang, H. M. Yang, K. Cui, J. H. Yu, *ACS Nano* **2023**, *17*, 13418.
[44] Y. B. Leng, Z. Y. Lv, S. M. Huang, P. Xie, H. X. Li, S. R. Zhu, T. Sun, Y. Zhou, Y. B. Zhai, Q. X. Li, G. L. Ding, Y. Zhou, S.-T. Han, *Adv. Mater.* **2024**, *36*, 2411225.
[45] T. T. Liu, X. M. Liu, Y. S. Feng, C. J. Yao, *Mater. Today Chem.* **2023**, *34*, 101788.
[46] S. Mohanty, A. M. Kaczmarek, *Chem. Soc. Rev.* **2022**, *51*, 6893.
[47] S. Singh, V. Takhar, S. H. Nannuri, S. D. George, R. Banerjee, S. K. Misra, *ACS Appl. Nano Mater.* **2023**, *6*, 10441.
[48] Y. Wang, Y. R. Wang, H. M. Zhong, L. H. Xiong, J. Y. Song, X. Y. Zhang, T. He, X. Y. Zhou, L. Li, D. S. Zhen, *J. Mater. Chem. B* **2024**, *12*, 5024.
[49] Y. Zhou, S.-T. Han, X. Chen, F. Wang, Y. B. Tang, V. A. L. Roy, *Nat. Commun.* **2014**, *8*, 4720.
[50] K. M. Du, J. Feng, X. Gao, H. J. Zhang, *Light: Sci. Appl.* **2022**, *11*, 222.
[51] R. C. Lv, M. Raab, Y. X. Wang, J. Tian, J. Lin, P. N. Prasad, *Coord. Chem. Rev.* **2022**, *460*, 214486.
[52] H. L. Wei, W. L. Zheng, X. Zhang, H. Suo, B. Chen, Y. Z. Wang, F. Wang, *Adv. Opt. Mater.* **2023**, *11*, 2201716.
[53] X. D. Zhao, Q. Liu, X. L. Li, H. Li, Z. R. Shen, H. M. Ji, T. Y. Ma, *Angew. Chem., Int. Ed.* **2023**, *62*, 202219214.
[54] M. Z. Sun, H. Dong, A. W. Dougherty, Q. Y. Lu, D. F. Peng, W. T. Wong, B. L. Huang, L. D. Sun, C. H. Yan, *Nano Energy* **2019**, *56*, 473.
[55] W. L. Wang, B. Chen, *Sci. Bull.* **2024**, *69*, 1809.
[56] L. Yan, J. S. Huang, Z. C. An, Q. Y. Zhang, B. Zhou, *Nat. Commun.* **2024**, *15*, 1923.
[57] Y. S. Feng, Z. Li, Q. Q. Li, J. Yuan, L. P. Tu, L. X. Ning, H. Zhang, *Light: Sci. Appl.* **2021**, *10*, 105.
[58] H. Wang, Z. He, K. Cai, L. M. Wei, Y. Xu, Y. Fu, M. M. Xing, Y. Tian, *Chem. Eng. J.* **2023**, *468*, 143558.
[59] R. R. Sun, M. C. Jia, X. Chen, F. Zhang, Z. Z. Ma, Y. Liu, J. B. Zhang, L. Y. Lian, Y. B. Han, M. Y. Li, D. W. Yang, X. J. Li, Y. Zhang, C. X. Shan, Z. F. Shi, *Laser Photonics Rev.* **2024**, *18*, 2301028.
[60] J. S. Huang, L. Yan, Z. C. An, H. P. Wei, C. Wang, Q. Y. Zhang, B. Zhou, *Adv. Mater.* **2024**, *36*, 2310524.
[61] N. Dubey, S. Chandra, *J. Rare Earths* **2022**, *40*, 1343.
[62] Y. Y. Niu, Z. H. Bao, Y. Q. Gao, M. C. Guo, J. Y. Liu, J. J. Shao, M. Lu, Z. Yuan, X. J. Xie, *J. Rare Earths* **2024**, *42*, 947.
[63] X. Zheng, R. K. Kankala, C. G. Liu, Y. Wen, S. B. Wang, A. Z. Chen, Y. Zhang, *Adv. Opt. Mater.* **2022**, *10*, 2200167.
[64] X. Chen, D. F. Peng, Q. Ju, F. Wang, *Chem. Soc. Rev.* **2015**, *44*, 1318.
[65] X. Cheng, J. Luo, F. Rosei, *Nano Mater. Sci.* **2024**.
[66] A. Skripka, M. Lee, X. Qi, J. A. Pan, H. R. Yang, C. Lee, P. J. Schuck, B. E. Cohen, D. Jaque, E. M. Chan, *Nano Lett.* **2023**, *23*, 7100.
[67] Y. S. Liang, Z. M. Zhu, S. Q. Qiao, X. Guo, R. Pu, H. Tang, H. C. Liu, H. Dong, T. T. Peng, L. D. Sun, E. E. Widengren, Q. Q. Zhan, *Nat. Nanotechnol.* **2022**, *17*, 524.
[68] H. Wu, B. X. Pan, Q. Zhao, C. Y. Wang, R. Pu, C. Liu, Z. H. Chen, Z. W. Luo, J. Huang, W. Wei, T. S. Chen, Q. Q. Zhan, *Adv. Photonics* **2024**, *6*, 056010.
[69] C. Lee, E. Z. Xu, K. W. C. Kwock, A. Teitelboim, Y. W. Liu, H. S. Park, B. Ursprung, M. E. Ziffer, Y. Karube, N. Fardian-Melamed, C. C. S. Pedroso, J. Kim, S. D. Pritzl, S. H. Nam, T. Lohmueller, J. S. Owen, P. Ercius, Y. D. Suh, B. E. Cohen, E. M. Chan, P. J. Schuck, *Nature* **2023**, *618*, 951.
[70] M. Dudek, M. Szalkowski, M. Misiak, M. Cwierzona, A. Skripka, Z. Korczak, D. Piatkowski, P. Wozniak, R. Lisiecki, P. Goldner, S. Mackowski, E. M. Chan, P. J. Schuck, A. Bednarkiewicz, *Adv. Opt. Mater.* **2022**, *10*, 2201052.
[71] C. Y. Wang, Z. Z. Wen, R. Pu, B. X. Pan, B. J. Wang, K. Z. Zheng, Y. Y. Du, Q. Q. Zhan, *Adv. Mater.* **2024**, *36*, 2307848.
[72] Z. D. Lei, X. Ling, Q. S. Mei, S. Fu, J. Zhang, Y. Zhang, *Adv. Mater.* **2020**, *32*, 1906225.
[73] J. S. Huang, L. Yan, S. B. Liu, N. Song, Q. Y. Zhang, B. Zhou, *Adv. Funct. Mater.* **2021**, *31*, 2009796.
[74] A. Schroter, S. Märkl, N. Weitzel, T. Hirsch, *Adv. Funct. Mater.* **2022**, *32*, 2113065.
[75] B. Zhou, L. Yan, J. S. Huang, X. L. Liu, L. L. Tao, Q. Y. Zhang, *Nat. Photonics* **2020**, *14*, 760.
[76] Y. Zhang, R. Wen, J. Hu, D. Guan, X. Qiu, Y. Zhang, D. S. Kohane, Q. Liu, *Nat. Commun.* **2022**, *13*, 5927.
[77] T. Sheng, M. Xu, Q. Li, Y. H. Wu, J. Zhang, J. L. Liu, X. H. Zhu, Y. Zhang, *Mater. Today Phys.* **2021**, *20*, 100451.
[78] X. W. Cheng, J. Zhou, J. Y. Yue, Y. Wei, C. Gao, X. J. Xie, L. Huang, *Chem. Rev.* **2022**, *122*, 15998.
[79] T. Liang, Q. R. Wang, Z. Li, P. P. Wang, J. J. Wu, M. M. Zuo, Z. H. Liu, *Adv. Funct. Mater.* **2020**, *30*, 1910765.
[80] W. Zhang, W. Zheng, P. Huang, D. F. Yang, Z. Q. Shao, X. Y. Chen, *Aggregate* **2024**, *5*, 558.
[81] Y. R. Guo, R. B. Zou, F. F. Si, W. L. Liang, T. Y. Zhang, Y. Y. Chang, X. S. Qiao, J. H. Zhao, *Food Chem.* **2021**, *335*, 127609.
[82] Q. Liu, B. Wu, M. Y. Li, Y. Y. Huang, L. L. Li, *Adv. Sci.* **2022**, *9*, 2103911.
[83] K. Park, K. Jung, S. J. Kwon, H. S. Jang, D. Byun, I. K. Han, H. Ko, *Adv. Funct. Mater.* **2016**, *26*, 7836.
[84] D. Mendez-Gonzalez, S. Melle, O. G. Calderón, M. Laurenti, E. Cabrera-Granado, A. Egatz-Gómez, E. López-Cabarcos, J. Rubio-Retama, E. Díaz, *Nanoscale* **2019**, *11*, 13832.
[85] J. Lee, B. Yoo, H. Lee, G. D. Cha, H. S. Lee, Y. Cho, S. Y. Kim, H. Seo, W. Lee, D. Son, M. Kang, H. M. Kim, Y. I. Park, T. Hyeon, D. H. Kim, *Adv. Mater.* **2017**, *29*, 1603169.
[86] N. N. Wang, Z. H. Li, W. Liu, T. Deng, J. F. Yang, R. H. Yang, J. S. Li, *ACS Appl. Mater. Interfaces* **2019**, *11*, 26684.
[87] Z. Q. Li, X. C. Zou, F. Shi, R. Liu, Y. Yagci, *Nat. Commun.* **2019**, *10*, 3560.
[88] Y. Q. Song, M. Chen, L. Han, Z. Y. Yan, L. Q. Pan, K. Tu, *Anal. Chim. Acta* **2023**, *1239*, 340751.
[89] F. Zhao, J. L. Hu, D. M. Guan, J. Y. Liu, X. B. Zhang, H. Ling, Y. X. Zhang, Q. Liu, *Adv. Mater.* **2023**, *35*, 2304907.

[90] A. Gupta, S. Ghosh, M. K. Thakur, J. J. Zhou, K. Ostrikov, D. Y. Jin, S. Chattopadhyay, *Prog. Mater. Sci.* **2021**, *121*, 100838.
[91] L. F. Ruan, Y. Zhang, *Nat. Commun.* **2021**, *12*, 219.
[92] L. T. Zhang, M. L. Liu, Z. L. Fang, Q. Ju, *Coord. Chem. Rev.* **2022**, *468*, 214641.
[93] M. M. Zhang, X. Wang, S. S. Liu, T. Riaz, Q. S. Chen, Q. Ouyang, *Biosens. Bioelectron.* **2024**, *254*, 116192.
[94] Y. C. Zhang, X. Xing, H. X. Zhao, J. Jiang, Y. Liu, Z. D. Lu, *Adv. Opt. Mater.* **2023**, *11*, 2201841.
[95] M. Zeng, S. Singh, Z. Hens, J. Liu, F. Artizzu, R. Van Deun, *J. Mater. Chem. C* **2019**, *7*, 2014.
[96] F. Xu, Y. Sun, H. P. Gao, S. Y. Jin, Z. L. Zhang, H. F. Zhang, G. C. Pan, M. Kang, X. Q. Ma, Y. L. Mao, *ACS Appl. Mater. Interfaces* **2021**, *13*, 2674.
[97] F. Z. Lv, J. La, S. J. He, Y. J. Liu, Y. D. Huang, Y. Wang, W. X. Wang, *ACS Appl. Mater. Interfaces* **2022**, *14*, 54304.
[98] C. Gao, Y. D. Han, K. Zhang, T. Wei, Z. Jiang, Y. Wei, L. S. Yin, F. Piccinelli, C. Yao, X. J. Xie, M. Bettinelli, L. Huang, *Adv. Sci.* **2020**, *7*, 2002444.
[99] A. T. Hoang, L. H. Hu, B. J. Kim, T. T. N. Van, K. D. Park, Y. Jeong, K. Lee, S. Ji, J. Hong, A. K. Katiyar, B. Shong, K. Kim, S. Im, W. J. Chung, J. H. Ahn, *Nat. Nanotechnol.* **2023**, *18*, 1439.
[100] L. Luo, J. W. Gao, L. Zheng, L. Li, W. W. Li, M. Z. Xu, H. J. Jiang, Y. Li, H. Wu, H. J. Ji, X. Dong, R. Q. Zhao, Z. Liu, X. W. Wang, W. Huang, *Infomat* **2024**, *6*, 12605.
[101] D. D. Li, S. H. Yu, H. L. Jiang, *Adv. Mater.* **2018**, *30*, 1707377.
[102] Y. Xie, G. T. Sun, J. W. Li, L. N. Sun, *Adv. Funct. Mater.* **2023**, *33*, 2303663.
[103] T. H. Zhao, J. L. Han, Y. H. Shi, J. Zhou, P. F. Duan, *Adv. Mater.* **2021**, *33*, 2101797.
[104] A. V. Kesavan, M. P. Kumar, A. D. Rao, P. C. Ramamurthy, *Opt. Mater.* **2019**, *94*, 286.
[105] D. Mendez-Gonzalez, O. G. Calderón, S. Melle, J. González-Izquierdo, L. Banares, D. López-Díaz, M. M. Velázquez, E. López-Cabarcos, J. Rubio-Retama, M. Laurenti, *J. Colloid Interface Sci.* **2020**, *575*, 119.
[106] Y. Zeng, X. P. Hu, S. B. Cheng, X. F. Wu, S. P. Zhan, Y. X. Liu, *Ceram. Int.* **2024**, *50*, 13960.
[107] J. Y. Shang, Y. X. Wang, J. L. Wu, Z. H. Li, H. B. Xia, Y. H. Jing, X. Y. Liu, W. Xu, B. Dong, *J. Colloid Interface Sci.* **2024**, *678*, 283.
[108] G. D. Feng, J. Jiang, Y. R. Li, D. D. Xie, B. B. Tian, Q. Wan, *Adv. Funct. Mater.* **2021**, *31*, 2104327.
[109] H. Y. Yu, H. H. Wei, J. D. Gong, H. Han, M. X. Ma, Y. F. Wang, W. T. Xu, *Small* **2021**, *17*, 2000041.
[110] M. B. Lien, C. H. Liu, I. Y. Chun, S. Ravishankar, H. Nien, M. M. Zhou, J. A. Fessler, Z. H. Zhong, T. B. Norris, *Nat. Photonics* **2020**, *14*, 143.
[111] F. Y. Zhang, B. Yang, K. B. Zheng, S. Q. Yang, Y. J. Li, W. Q. Deng, R. X. He, *Nano-Micro Lett.* **2018**, *10*, 43.
[112] Z. Q. Li, T. T. Yan, X. S. Fang, *Nat. Rev. Mater.* **2023**, *8*, 587.
[113] W. J. Zhou, Y. Q. Shang, F. P. G. de Arquer, K. M. Xu, R. L. Wang, S. B. Luo, X. B. Xiao, X. Y. Zhou, R. M. Huang, E. H. Sargent, Z. J. Ning, *Nat. Electron.* **2020**, *3*, 251.
[114] S. C. Du, W. Lu, A. Ali, P. Zhao, K. Shehzad, H. W. Guo, L. L. Ma, X. M. Liu, X. D. Pi, P. Wang, H. H. Fang, Z. Xu, C. Gao, Y. P. Dan, P. H. Tan, H. T. Wang, C. T. Lin, J. Y. Yang, S. R. Dong, Z. Y. Cheng, E. P. Li, W. Y. Yin, J. K. Luo, B. Yu, T. Hasan, Y. Xu, W. D. Hu, X. F. Duan, *Adv. Mater.* **2017**, *29*, 1700463.
[115] S. H. Park, R. Su, J. Jeong, S.-Z. Guo, K. Qiu, D. Joung, F. Meng, M. C. McAlpine, *Adv. Mater.* **2018**, *30*, 1803980.
[116] Y. Zhang, Z. S. Qin, H. K. Gao, T. Y. Wang, C. Gao, X. T. Zhang, W. P. Hu, H. L. Dong, *Adv. Mater.* **2024**, *36*, 2404309.
[117] L. D. Han, L. Yan, C. X. Yu, Y. X. Liu, F. Wu, X. Zhang, X. Yao, C. Y. Li, J. H. Chen, X. S. Chen, J. M. Lan, *Microchem. J.* **2023**, *184*, 108196.
[118] M. Kataria, K. Yadav, G. Haider, Y. M. Liao, Y. R. Liou, S. Y. Cai, H. I. Lin, Y. H. Chen, C. R. P. Inbaraj, K. P. Bera, H. M. Lee, Y. T. Chen, W. H. Wang, Y. F. Chen, *ACS Photonics* **2018**, *5*, 2336.
[119] S. Ghosh, W. C. Chiang, M. Y. Fakhri, C. T. Wu, R. S. Chen, S. Chattopadhyay, *Nano Energy* **2020**, *67*, 104258.
[120] J. H. Wu, Z. W. Yang, C. Y. Qiu, Y. J. Zhang, Z. Q. Wu, J. L. Yang, Y. H. Lu, J. F. Li, D. X. Yang, R. Hao, E. P. Li, G. L. Yu, S. S. Lin, *Nanoscale* **2018**, *10*, 8023.
[121] Y. J. Zheng, Z. Xu, K. X. Shi, J. H. Li, X. Fang, Z. F. Jiang, X. Y. Chu, *J. Mater. Chem. C* **2024**, *12*, 18291.
[122] A. Gupta, D. K. Patel, S. Y. Lee, A. F. Rigosi, R. E. Elmquist, V. Adusumalli, C. T. Liang, Y. I. Park, *Adv. Funct. Mater.* **2022**, *32*, 2206496.
[123] J. A. La, H. S. Jang, J. Kim, J. Kang, T. Kang, G. Kang, H. Ko, *IEEE Sens. J.* **2024**, *24*, 27393.
[124] G. Q. Fang, Y. A. Ji, Q. Xiao, X. Y. Dong, J. L. Wu, J. X. Zou, Y. Z. Xu, W. Xu, B. Dong, *J. Mater. Chem. C* **2022**, *10*, 16430.
[125] H. F. Xie, Q. Pan, D. D. Wu, F. F. Qin, S. R. Chen, W. Sun, X. Yang, S. S. Chen, T. Q. Wu, J. M. Chi, Z. Q. Huang, H. D. Wang, Z. Y. Zhang, B. D. Chen, J. Carmeliet, M. Su, Y. L. Song, *ACS Nano* **2022**, *16*, 16563.
[126] S. Zhang, K. X. Guo, L. Sun, Y. Ni, L. Liu, W. L. Xu, L. Yang, W. T. Xu, *Adv. Mater.* **2021**, *33*, 2007350.
[127] Z. H. Long, Y. Zhou, Y. C. Ding, X. Qiu, S. Poddar, Z. Y. Fan, *Nat. Rev. Mater.* **2025**, *10*, 128.
[128] S. Kamaei, X. Liu, A. Saeidi, Y. F. Wei, C. Gastaldi, J. Brugger, A. M. Ionescu, *Nat. Electron.* **2023**, *6*, 658.
[129] G. D. Feng, Y. F. Liu, Q. X. Zhu, Z. Y. Feng, S. W. Luo, C. J. Qin, L. Q. Chen, Y. Xu, H. A. Wang, M. Zubair, K. Qu, C. Yang, S. L. Hao, F. Y. Yue, C. G. Duan, J. H. Chu, B. B. Tian, *Nat. Commun.* **2024**, *15*, 9701.
[130] G. J. Wu, B. B. Tian, L. Liu, W. Lv, S. Wu, X. D. Wang, Y. Chen, J. Y. Li, Z. Wang, S. Q. Wu, H. Shen, T. Lin, P. Zhou, Q. Liu, C. G. Duan, S. T. Zhang, X. J. Meng, S. W. Wu, W. D. Hu, X. R. Wang, J. H. Chu, J. L. Wang, *Nat. Electron.* **2020**, *3*, 43.
[131] M. K. Kim, J. S. Lee, *Adv. Mater.* **2020**, *32*, 1907826.
[132] L. Sun, S. D. Qu, W. T. Xu, *Mater. Horiz.* **2023**, *10*, 5753.
[133] X. Yang, J. Huang, J. J. Li, Y. Q. Zhao, H. F. Li, Z. Y. Yu, S. Y. Gao, R. Cao, *Adv. Mater.* **2024**, *36*, 2313608.
[134] B. W. Zhang, T. Bai, L. Han, S. A. Che, Y. Y. Duan, *Adv. Mater.* **2024**, *36*, 2403142.
[135] S. D. Qu, L. Sun, S. Zhang, J. Q. Liu, Y. Li, J. C. Liu, W. T. Xu, *Nat. Commun.* **2023**, *14*, 7181.
[136] J. D. Gong, H. H. Wei, Y. Ni, S. Zhang, Y. Du, W. T. Xu, *Mater. Today Phys.* **2021**, *21*, 100540.
[137] Y. F. Pei, Z. Q. Li, B. Li, Y. Zhao, H. He, L. Yan, X. Y. Li, J. J. Wang, Z. Zhao, Y. Sun, Z. Y. Zhou, J. H. Zhao, R. Guo, J. S. Chen, X. B. Yan, *Adv. Funct. Mater.* **2022**, *32*, 2203454.
[138] W. H. Yang, H. Kan, G. Z. Shen, Y. Li, *Adv. Funct. Mater.* **2024**, *34*, 2312885.
[139] Z. Y. Wang, L. Y. Wang, Y. M. Wu, L. Y. Bian, M. Nagai, R. L. Jv, L. H. Xie, H. F. Ling, Q. Li, H. Bian, M. D. Yi, N. E. Shi, X. G. Liu, W. Huang, *Adv. Mater.* **2021**, *33*, 2104370.
[140] L. Yin, C. Han, Q. T. Zhang, Z. Y. Ni, S. Y. Zhao, K. Wang, D. S. Li, M. S. Xu, H. Q. Wu, X. D. Pi, D. R. Yang, *Nano Energy* **2019**, *63*, 103859.
[141] K. C. Kwon, J. H. Baek, K. Hong, S. Y. Kim, H. W. Jang, *Nano-Micro Lett.* **2022**, *14*, 58.
[142] J. Tang, C. L. He, J. S. Tang, K. Yue, Q. T. Zhang, Y. Z. Liu, Q. Q. Wang, S. P. Wang, N. Li, C. Shen, Y. C. Zhao, J. Y. Liu, J. H. Yuan, Z. Wei, J. W. Li, K. Watanabe, T. Taniguchi, D. S. Shang, S. G. Wang, W. Yang, R. Yang, D. X. Shi, G. Y. Zhang, *Adv. Funct. Mater.* **2021**, *31*, 2011083.

[143] Y. Q. Liu, E. L. Li, X. M. Wang, Q. Z. Chen, Y. L. Zhou, Y. Y. Hu, G. X. Chen, H. P. Chen, T. L. Guo, *Nano Energy* **2020**, *78*, 105403.
[144] I. J. Kim, M. K. Kim, J. S. Lee, *Nat. Commun.* **2023**, *13*, 504.
[145] L. Wang, H. T. Wang, J. Liu, Y. R. Wang, H. Shao, W. Li, M. D. Yi, H. F. Ling, L. H. Xie, W. Huang, *Adv. Mater.* **2024**, *36*, 2403538.
[146] J. L. Meng, T. Y. Wang, Z. Y. He, L. Chen, H. Zhu, L. Ji, Q. Q. Sun, S. J. Ding, W. Z. Bao, P. Zhou, D. W. Zhang, *Mater. Horiz.* **2021**, *8*, 538.
[147] L. Liu, G. Peng, M. R. Zhang, J. D. Dou, C. S. Liu, T. Shi, H. Huang, C. L. Wang, H. He, Z. J. Chen, Y. Chai, J. L. Wang, X. M. Zou, L. Liao, J. L. Wang, P. Zhou, *Adv. Sci.* **2024**, *11*, 2408210.
[148] K. M. Song, J.-S. Jeong, B. Pan, X. Zhang, J. Xia, S. Cha, T.-E. Park, K. Kim, S. Finizio, J. Raabe, J. Chang, Y. Zhou, W. Zhao, W. Kang, H. Ju, S. Woo, *Nat. Electron.* **2020**, *3*, 148.
[149] X. X. Liu, S. Y. Wang, Z. Y. Di, H. Q. Wu, C. S. Liu, P. Zhou, *Adv. Sci.* **2023**, *10*, 2301851.
[150] Y. C. Cai, F. Wang, X. M. Wang, S. H. Li, Y. R. Wang, J. Yang, T. Yan, X. Y. Zhan, F. M. Wang, R. Q. Cheng, J. He, Z. X. Wang, *Adv. Funct. Mater.* **2023**, *33*, 2212917.
[151] Z. M. Wei, *Nat. Electron.* **2022**, *5*, 715.
[152] J. Zhou, T. Y. Zhao, X. Y. Shu, L. Liu, W. N. Lin, S. H. Chen, S. Shi, X. B. Yan, X. G. Liu, J. S. Chen, *Adv. Mater.* **2021**, *33*, 2103672.
[153] J. W. Qiu, J. L. Li, W. H. Li, K. Wang, S. Q. Zhang, C. H. Suk, C. X. Wu, X. T. Zhou, Y. G. Zhang, T. L. Guo, T. W. Kim, *ACS Nano* **2024**, *18*, 31632.
[154] G. M. Cao, P. Meng, J. G. Chen, H. S. Liu, R. J. Bian, C. Zhu, F. C. Liu, Z. Liu, *Adv. Funct. Mater.* **2021**, *31*, 2005443.
[155] S. Choi, J. Yang, G. Wang, *Adv. Mater.* **2020**, *32*, 2004659.
[156] Y. Q. Liu, W. Y. Yang, Y. J. Yan, X. M. Wu, X. M. Wang, Y. L. Zhou, Y. Y. Hu, H. P. Chen, T. L. Guo, *Nano Energy* **2020**, *75*, 104930.
[157] Y. Park, M. K. Kim, J. S. Lee, *J. Mater. Chem. C* **2021**, *9*, 5396.
[158] S. Ham, J. Jang, D. Koo, S. Gi, D. Kim, S. Jang, N. D. Kim, S. Bae, B. Lee, C. H. Lee, G. Wang, *Nano Energy* **2024**, *124*, 109435.
[159] D. Cai, Y. B. Liu, J. Y. Wang, T. C. Zhao, M. Shen, F. J. Zhang, Y. D. Jiang, D. Gu, *Adv. Funct. Mater.* **2024**, *34*, 2314660.
[160] B. J. Dang, T. Zhang, X. L. Wu, K. Q. Liu, R. Huang, Y. C. Yang, *Nat. Electron.* **2024**, *7*, 991.
[161] C. S. Chen, Y. Q. Zhou, L. Tong, Y. Pang, J. B. Xu, *Adv. Mater.* **2025**, *37*, 2400332.
[162] M. Vasilopoulou, A. B. Yusoff, Y. Chai, M. A. Kourtis, T. Matsushima, N. Gasparini, R. Du, F. Gao, M. K. Nazeeruddin, T. D. Anthopoulos, Y. Y. Noh, *Nat. Electron.* **2023**, *6*, 949.
[163] O. Lee, T. Wei, K. D. Stenning, J. C. Gartside, D. Prestwood, S. Seki, A. Aqeel, K. Karube, N. Kanazawa, Y. Taguchi, C. Back, Y. Tokura, W. R. Branford, H. Kurebayashi, *Nat. Mater.* **2024**, *23*, 79.
[164] J. Park, T. H. Kim, O. Kwon, M. Ismail, C. Mahata, Y. Kim, S. Kim, S. Kim, *Nano Energy* **2022**, *104*, 107886.
[165] X. P. Liang, J. S. Tang, Y. N. Zhong, B. Gao, H. Qian, H. Q. Wu, *Nat. Electron.* **2024**, *7*, 193.
[166] S. Wakabayashi, T. Arie, S. Akita, K. Nakajima, K. Takei, *Adv. Mater.* **2022**, *34*, 2201663.
[167] Y. N. Zhong, J. S. Tang, X. Y. Li, X. P. Liang, Z. W. Liu, Y. J. Li, Y. Xi, P. Yao, Z. Q. Hao, B. Gao, H. Qian, H. Q. Wu, *Nat. Electron.* **2022**, *5*, 672.
[168] M. J. Pei, Y. Zhu, S. Y. Liu, H. Y. Cui, Y. T. Li, Y. Yan, Y. Li, C. J. Wan, Q. Wan, *Adv. Mater.* **2023**, *35*, 2305609.
[169] M. R. Lian, C. S. Gao, Z. Y. Lin, L. T. Shan, C. Chen, Y. Zou, E. P. Cheng, C. F. Liu, T. L. Guo, W. Chen, H. P. Chen, *Light: Sci. Appl.* **2024**, *13*, 179.
[170] Y. Zhang, X. H. Zhu, Y. Zhang, *ACS Nano* **2021**, *15*, 3709.
[171] A. A. Ansari, V. K. Thakur, G. Chen, *Coord. Chem. Rev.* **2021**, *436*, 213821.
[172] C. Schiattarella, S. Romano, L. Sirleto, V. Mocella, I. Rendina, V. Lanzio, F. Riminucci, A. Schwartzberg, S. Cabrini, J. Chen, L. Liang, X. Liu, G. Zito, *Nature* **2024**, *626*, 765.
[173] D. B. L. Teh, A. Bansal, C. Chai, T. B. Toh, R. A. J. Tucker, G. G. L. Gammad, Y. Yeo, Z. Lei, X. Zheng, F. Yang, J. S. Ho, N. Bolem, B. C. Wu, M. K. Gnanasammandhan, L. Hooi, G. S. Dawe, C. Libedinsky, W.-Y. Ong, B. Halliwell, E. K.-H. Chow, K.-L. Lim, Y. Zhang, B. K. Kennedy, *Adv. Mater.* **2020**, *32*, 2001459.
[174] A. A. Ansari, A. K. Parchur, G. Chen, *Coord. Chem. Rev.* **2022**, *457*, 214423.
[175] K. Roy, A. Jaiswal, P. Panda, *Nature* **2019**, *575*, 607.
[176] Y. Y. Fu, Y. Zhou, X. D. Huang, B. Y. Dong, F. W. Zhuge, Y. Li, Y. H. He, Y. Chai, X. S. Miao, *Adv. Funct. Mater.* **2022**, *32*, 2111996.
[177] S. R. Nason, A. K. Vaskov, M. S. Willsey, E. J. Welle, H. An, P. P. Vu, A. J. Bullard, C. S. Nu, J. C. Kao, K. V. Shenoy, T. Jang, H. S. Kim, D. Blaauw, P. G. Patil, C. A. Chestek, *Nat. Biomed. Eng.* **2020**, *4*, 973.
[178] S. K. Nath, S. K. Das, S. K. Nandi, C. Xi, C. V. Marquez, A. Rúa, M. Uenuma, Z. R. Wang, S. Q. Zhang, R. J. Zhu, J. Eshraghian, X. Sun, T. Lu, Y. Bian, N. Syed, W. W. Pan, H. Wang, W. Lei, L. Fu, L. Faraone, Y. Liu, R. G. Elliman, *Adv. Mater.* **2024**, *36*, 2400904.
[179] H. Y. Bian, Y. Y. Goh, Y. X. Liu, H. F. Ling, L. H. Xie, X. G. Liu, *Adv. Mater.* **2021**, *33*, 2006469.
[180] Y. Li, X. N. Ru, M. Yang, Y. H. Zheng, S. Yin, C. J. Hong, F. G. Peng, M. H. Qu, C. W. Xue, J. X. Lu, L. Fang, C. Su, D. F. Chen, J. H. Xu, C. Yan, Z. G. Li, X. X. Xu, Z. P. Shao, *Nature* **2024**, *626*, 105.

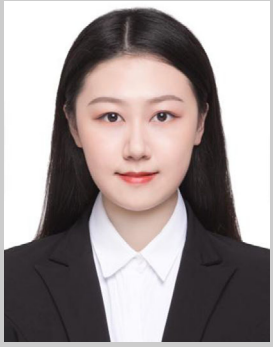

Sunyingyue Geng received her bachelor's degree in microelectronics science and engineering and master's degree in materials engineering from Qingdao University. She is presently a Ph.D. student at the College of Electronics and Information Engineering, Shenzhen University. Her research interest includes novel neuromorphic devices and optoelectronic devices.

Hangfei Li received his bachelor's degree in microelectronics science and engineering and master's degree in materials engineering from Qingdao University. He is presently a Ph.D. student at the College of Electronics and Information Engineering, Shenzhen University. His research interest includes novel memristor and optoelectronic devices.

Yongbiao Zhai is currently an Assistant Professor at Shenzhen University. He received his Ph.D. degree from the University of China Academy of Sciences in 2017. His research interests are focused on the preparation of nanoscale devices and their application in memory devices and artificial synapse devices.

Su-Ting Han is currently an associate professor in the Department of Applied Biology and Chemical Technology at the Hong Kong Polytechnic University. She received Ph.D. in physics and materials science from the City University of Hong Kong in 2014 and became a postdoctoral researcher. She joined Shenzhen University in 2016 and was promoted to full professor (tenured) in 2021 and then distinguished professor in 2022. She was visiting professor in the Department of Electrical Engineering and Computer Science at the University of Michigan, USA, in 2019. Her research interest includes flash memory, memristor, neuromorphic devices, and in-memory computing systems.